



RESEARCH ARTICLE

10.1002/2016JD025304

Key Points:

- Atmospheric and surface urban heat islands (UHIs) were compared in Beijing
- The nighttime UHIs referenced to rural croplands exhibited obvious seasonal cycles but not for those referenced to mountainous forests
- The impervious surface ratio explains 49%–54% of the nighttime atmospheric UHIs and 31%–38% of the daytime surface UHI

Supporting Information:

- Supporting Information S1

Correspondence to:

K. Wang,
kwang@bnu.edu.cn

Citation:

Wang, K., S. Jiang, J. Wang, C. Zhou, X. Wang, and X. Lee (2017), Comparing the diurnal and seasonal variabilities of atmospheric and surface urban heat islands based on the Beijing urban meteorological network, *J. Geophys. Res. Atmos.*, 122, 2131–2154, doi:10.1002/2016JD025304.

Received 2 MAY 2016

Accepted 3 FEB 2017

Accepted article online 6 FEB 2017

Published online 17 FEB 2017

Comparing the diurnal and seasonal variabilities of atmospheric and surface urban heat islands based on the Beijing urban meteorological network

Kaicun Wang^{1,2} , Shaojing Jiang^{1,2} , Jiankai Wang³ , Chunlue Zhou^{1,2} , Xiaoyan Wang^{1,2} , and Xuhui Lee^{4,5}

¹College of Global Change and Earth System Science, Beijing Normal University, Beijing, China, ²Joint Center for Global Change Studies, Beijing, China, ³Chinese Academy of Meteorological Sciences, Beijing, China, ⁴Yale-NUIST Center on Atmospheric Environment, Nanjing University of Information, Science and Technology, Nanjing, China, ⁵School of Forestry and Environmental Studies, Yale University, New Haven, Connecticut, USA

Abstract This study compared the diurnal and seasonal cycles of atmospheric and surface urban heat islands (UHIs) based on hourly air temperatures (T_a) collected at 65 out of 262 stations in Beijing and land surface temperature (T_s) derived from Moderate Resolution Imaging Spectroradiometer in the years 2013–2014. We found that the nighttime atmospheric and surface UHIs referenced to rural cropland stations exhibited significant seasonal cycles, with the highest in winter. However, the seasonal variations in the nighttime UHIs referenced to mountainous forest stations were negligible, because mountainous forests have a higher nighttime T_s in winter and a lower nighttime T_a in summer than rural croplands. Daytime surface UHIs showed strong seasonal cycles, with the highest in summer. The daytime atmospheric UHIs exhibited a similar but less seasonal cycle under clear-sky conditions, which was not apparent under cloudy-sky conditions. Atmospheric UHIs in urban parks were higher in daytime. Nighttime atmospheric UHIs are influenced by energy stored in urban materials during daytime and released during nighttime. The stronger anthropogenic heat release in winter causes atmospheric UHIs to increase with time during winter nights, but decrease with time during summer nights. The percentage of impervious surfaces is responsible for 49%–54% of the nighttime atmospheric UHI variability and 31%–38% of the daytime surface UHI variability. However, the nighttime surface UHI was nearly uncorrelated with the percentage of impervious surfaces around the urban stations.

1. Introduction

Although urban areas occupy less than 0.5% of the Earth's land surface [Schneider *et al.*, 2009], they contain more than half of the global population (<http://esa.un.org/unpd/wup/Publications/Files/WUP2014-Highlights.pdf>). The term "urban heat island" (UHI) refers to the phenomenon of urban areas being warmer than surrounding rural areas. UHI occurs in almost all urban areas [Stewart and Oke, 2012]. The possible causes of UHI have been outlined [Oke, 1982; Stewart and Oke, 2012]: (1) greater absorption of solar radiation in the urban areas, (2) lower efficiency of longwave radiation emission in the urban areas, (3) energy storage by buildings and paved surfaces in the urban areas and its release, (4) lower evaporative cooling in urban areas due to lower vegetation coverage, and (5) anthropogenic heat release in urban areas. UHIs play important roles in local and regional climates [Chen *et al.*, 2015; Rosenfeld, 2000; Zhou *et al.*, 2004], air pollution [Sarrat *et al.*, 2006], and human health [Rydin *et al.*, 2012]. There has been increasing interest in the effect of UHIs on the homogeneity of air temperature (T_a) observations [Jones and Lister, 2009; Karl *et al.*, 1988; Karl and Jones, 1989; Parker, 2010; Ren and Zhou, 2014].

The first study of UHIs dates to the early 19th century [Howard, 1833]; since that time, UHIs have been extensively investigated in cities of different sizes and climates [Arnfield, 2003; Chow *et al.*, 2012; Oke *et al.*, 1991]. Air temperature (T_a) data collected at urban and rural weather stations have long been compared to study atmospheric UHIs [Oke, 1973]. In general, nighttime atmospheric UHIs are stronger than daytime ones [Oke and Cleugh, 1987], atmospheric UHIs in high-rise city centers are stronger than those in residential suburbs, and atmospheric UHIs can be completely eliminated in city parks [Parker, 2010; Peterson, 2003].

©2017. The Authors.

This is an open access article under the terms of the Creative Commons Attribution-NonCommercial-NoDerivs License, which permits use and distribution in any medium, provided the original work is properly cited, the use is non-commercial and no modifications or adaptations are made.

Urban areas are complex and heterogeneous environments; therefore, measurements from single urban monitoring stations do not provide sufficient detail for urban climate research and decision-making applications [Oke, 2008]. Monitoring UHIs with dense sensor networks can improve understanding of the urban environment [Chapman et al., 2013; Muller et al., 2013a; Azevedo et al., 2016]. With a highly dense urban monitoring network, Bassett et al. [2016] studied the effect of urban heat advection on UHIs in Birmingham, UK. The data from a dense urban meteorological network were analyzed to show the spatial heterogeneity and temporal variability of atmospheric UHI in the Twin Cities (Minneapolis-St. Paul, MN, USA) [Smoliak et al., 2015]. The data from the Oklahoma City urban meteorological network (36 stations) in 2009 and 2010 were used to investigate the spatial variability of UHIs and their results do not support the roughness warming theory to explain atmospheric UHI [Hu et al., 2016]. T_a at 64 stations of the Beijing meteorological urban network has been used to analyze the spatial and temporal characteristics of UHIs over the densely populated areas [Yang et al., 2013].

Satellite-derived land surface temperature (T_s) data have also been employed to investigate the surface UHI phenomenon [Jin and Shepherd, 2005; Price, 1979; Roth et al., 1989; Voogt and Oke, 2003]. Satellite T_s data enable easy assessments of surface UHIs across cities worldwide [Clinton and Gong, 2013; Imhoff et al., 2010; Mertes et al., 2015; Peng et al., 2012]. Satellite data also facilitate analyses of the spatial variability of surface UHIs within cities [Weng, 2009; Weng et al., 2004].

Significant differences between atmospheric and surface UHIs have been reported [Arnfield, 2003]. For example, surface UHIs are the highest during summer daytime [Imhoff et al., 2010], whereas atmospheric UHIs are the strongest during winter nighttime [Oke and Cleugh, 1987]. Furthermore, surface UHIs exhibit greater dependencies on background climates [Zhao et al., 2014], and their intensities can be negative in arid areas [Price, 1979], i.e., urban areas can be cooler than the surrounding rural areas; such a situation is referred to as an “urban cool island” [Theeuwes et al., 2015]. One reason for such debates is that studies on atmospheric UHIs based on T_a concentrate more on the nighttime, whereas studies of surface UHIs focus on the daytime [Weng et al., 2004; Zhao et al., 2014]. The cause of daytime surface UHIs may differ from that of nighttime surface UHIs [Peng et al., 2012].

Numerous studies have been conducted to study UHIs over Beijing, the majority focusing on surface UHIs derived from satellite-derived T_s data. Liu et al. [2016] showed that the surface UHI over Beijing is more obvious from May to October and claimed that the surface UHI is inconsistent with the atmospheric UHI; however, Y. Lu et al. [2014] demonstrated that temporal changes of surface and atmospheric UHIs have high consistency. Specifically, Sun et al. [2015] reported that surface UHIs agree well with atmospheric UHIs during nighttime, but they differ substantially during daytime in intensity or spatial pattern.

Changes in land cover, vegetation growth, and urban expansion with more compact structures are suggested as primary controlling factors of atmospheric and surface UHIs in Beijing. Xu and Liu [2015] observed that daytime (10:42 A.M., Beijing time) atmospheric UHIs, based on the calculated T_a with derived T_s from Landsat imagery on 26 July 2011, increased significantly with impervious surface coverage. Peng et al. [2016] suggested that urban landscape types such as built-up areas and barren land make the most significant contribution. Chen et al. [2014] also argued that the percentage of impervious surface is the most important factor determining surface UHIs and can account for 56% of the variance of surface UHIs. Feng et al. [2014] found that urban growth has little impact on surface UHIs. Choi et al. [2014] showed that surface UHIs over Beijing had a strong negative correlation with vegetation coverage during daytime, but such a relation was not observed during nighttime. Kuang et al. [2015] studied the relationship between surface UHIs and vegetation coverage over Beijing and argued that the city should upgrade the traditional low-rise residential areas to high-rise residential areas to reduce UHI intensity.

We have not identified any published study using both T_a and T_s data to directly compare these two types of UHIs over various types of city land cover and use. Additionally, both types of UHIs have important diurnal and seasonal cycles, which can reveal important information regarding the causes of the UHIs. To gain insight into the dynamics of UHIs and their determining factors, we investigated UHIs using hourly T_a observations collected at 262 stations in the Beijing urban meteorological network and T_s retrievals 4 times daily based on satellite observations made by the Moderate Resolution Imaging Spectroradiometer (MODIS) aboard the NASA Earth Observation System (EOS) Terra and Aqua polar orbit satellite platforms in the years 2013–2014. In this study, the diurnal and seasonal cycles of atmospheric and surface UHIs were compared

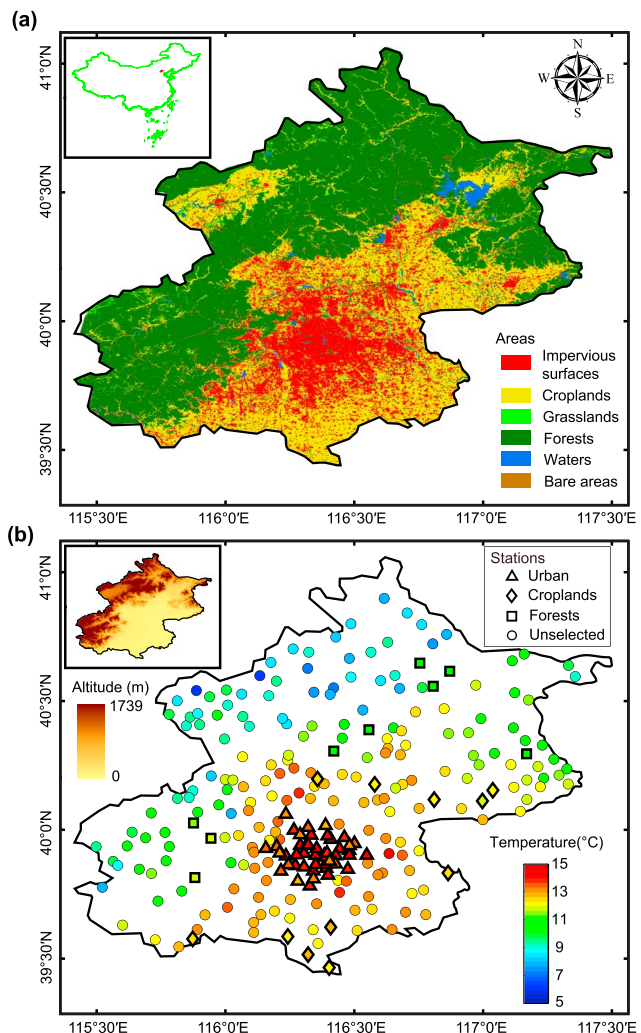


Figure 1. (a) Land cover types in 2013 over the Beijing metropolitan region based on Landsat satellite observations at 30 m resolution [Wang et al., 2015]. (b) Map of the 262 automatic weather stations and their annual mean air temperature (T_a) readings. The elevation of the study area is shown in the inset in Figure 1b (top left). We selected 45 urban stations in central urban areas to study atmospheric and surface UHIs and their dependence on the percentage of impervious surfaces of the urban stations. Furthermore, we selected 11 rural cropland stations and 9 mountainous forest stations as rural reference stations to investigate the impact of the selection of rural reference stations on the UHIs. Clearly, the 2 year annual mean T_a over the northwest is lower due to their higher surface elevation. To reduce this impact, we corrected the temperatures (including T_a and T_s) by assuming that they decreased with height at a rate of 0.6°C per 100 m. This correction was empirical and may have a large uncertainty.

studies [Parker, 2006, 2010; Pielke et al., 2007a; Pielke et al., 2007b] but is helpful in studying local environment, i.e., UHIs.

To better understand UHIs, researchers came up with different schemes for the deployment of urban meteorological stations. For example, Oke [2008] simply divided urban areas into seven homogenous regions to improve the siting of meteorological instruments in urban areas. The Beijing urban meteorological network AWS was deployed without changing the original land use in the urban areas (Figure 2), thus enabling UHI investigations for typical types of urban land cover. Approximately 300 AWSs have been deployed in the Beijing metropolitan region. The deployment of AWSs was relatively denser in primary urban districts

over different urban and rural land cover types. The dependency of the atmospheric and surface UHIs on the rural background (i.e., rural croplands or mountainous forests) and their relation with the percentage of impervious surfaces of urban stations were carefully examined. From these analyses, the differences in their variabilities were demonstrated, and their determining factors were inferred.

2. Data and Study Area

2.1. Beijing Urban Meteorological Network

Beijing, the capital of the People's Republic of China, is located in the northern portion of the North China Plain (Figure 1a). The city is situated on a plain at an altitude of 20–60 m above sea level (Figure 1b). Mountains are situated in the northern and western regions of the city, with elevations up to 1500 m. The Beijing metropolitan area had a permanent resident population of 21 million in 2013. Its annual energy consumption in 2013 was 6.7×10^7 t of standard coal energy. Beijing experiences a typical monsoon climate with approximately 500 mm of total annual precipitation, and most rainfall occurs during the wet season (June to September).

Generally, a typical weather station should be ideally established in an open grassland away from tall buildings with the size ranging from 10 m × 7 m to 25 m × 25 m according to the World Meteorological Organization guide. Satisfying this requirement of location and size for an urban automatic weather station (AWS) can be difficult. Failure to meet this requirement may introduce biases into large-scale climate change



Figure 2. (a1–a4) Photos and (b1–b4) Google Earth maps of four selected urban AWSs. The warning tower station, in which an air temperature sensor was deployed on a 16.6-m high meteorological early warning tower on the street (Figures 2a1 and 2b1). The Tian'anmen Square station, which is located in a small green belt in Tian'anmen Square (Figures 2a2 and 2b2). The China Meteorological Administration station, which is located in a standard weather station but surrounded by high buildings (Figures 2a3 and 2b3). The Temple of Heaven Park station, which is located in the Temple of Heaven Park (Figures 2a4 and 2b4).

(Figure 1), and most AWSs were set in green belts in dense-constructed areas (Figure 2). The ground area size of each AWS depends on the regional background of its deployment, with the maximum area reaching 25 m × 25 m, and there may be no fence around some urban AWSs because of the complex situation.

In general, two types of AWS system were used in the Beijing urban meteorological network: Vaisala MAWS301 and CAWS600. The two types of AWS system use similar air temperature sensors, which have an accuracy of $\pm 0.3^\circ\text{C}$ at 20°C . The AWSs record minute averages of air temperature, relative humidity, atmospheric pressure, wind speed and direction, and precipitation at 1.5 m above ground. AWS data

with temporal resolutions of 1 min, 5 min, and 1 h were transferred to a data center, and extensive quality control procedures were performed, including checks of the plausible values, time consistency, internal consistency, historical values, and spatial distribution [Dou *et al.*, 2008; L. Lu *et al.*, 2014]. In 2013 and 2014, there were 262 AWSs in metropolitan Beijing that were functioning well and providing data (Figure 1).

Because of the growing use of urban meteorological data, it is imperative that the network of AWSs is of high quality and implemented to a high standard [Muller *et al.*, 2013a]. Studies have shown that the T_a data collected by the Beijing urban meteorological network AWSs are reliable [Yang *et al.*, 2011]. Compared with 1 min and 5 min data, the hourly data are of the highest quality and quite reliable, and we therefore used hourly T_a data in this study [Yang *et al.*, 2011]. The major factor that affects the accuracy of T_a is missing data [L. Lu *et al.*, 2014]. The total data missing rate of T_a of the Beijing urban meteorological network is 3.8%, and the data missing rate is generally less than 1% for most stations [Yang *et al.*, 2011]. Questionable data were flagged and not included in this study.

2.2. MODIS Satellite-Derived Land Surface Temperatures

Satellite-derived T_s data have been extensively applied to studies of UHIs since the late 1970s and, in particular, to studies of UHIs during the daytime [Gallo *et al.*, 1995; Kidder and Wu, 1987; Price, 1979; Roth *et al.*, 1989]. Satellite T_s data with high spatial resolution have the advantage of reflecting UHI texture information [Gluch *et al.*, 2006], whereas satellite T_s data with high temporal resolution and low spatial resolution have the advantage of characterizing the seasonal variability in UHIs [Pu *et al.*, 2006]. In this study, we employed MODIS-derived T_s data to investigate the diurnal and seasonal cycles of the UHIs in the Beijing metropolitan area. The MODIS instruments that are onboard NASA EOS satellite platforms observe Beijing 4 times per day at approximately 01:30, 10:30, 13:30, and 22:30 local Beijing time.

In this study, we employed the T_s product at a 1 km resolution, which was retrieved via a split-window algorithm by using the land-cover-type-based surface emissivity [Wan and Dozier, 1996]. A MODIS pixel has a spatial resolution of 1 km² at nadir; however, the resolution can easily increase to several km² at wide scan angles from 0° (nadir) to 65° [Justice *et al.*, 1998; Wolfe *et al.*, 2002]. Although this T_s product was resampled to 1 km², it may convey T_s information over a much larger area. Validation studies have demonstrated the reasonable accuracy of this T_s product, which has an error standard deviation of 1–2°C [Wan *et al.*, 2002; Wang and Liang, 2009; Wang *et al.*, 2007a].

The MODIS T_s product has been employed to analyze UHIs on regional and global scales [Clinton and Gong, 2013; Mertes *et al.*, 2015; Wang *et al.*, 2007b]. The view zenith angle of MODIS varies from 0° to 65° [Justice *et al.*, 1998; Wolfe *et al.*, 2002]. The anisotropic effects of longwave radiation emission can be important for high view zenith angle (i.e., >55°) [Kribus *et al.*, 2003; McAtee *et al.*, 2003]. However, studies have shown that the anisotropic effect in urban and rural areas is not an important issue when using MODIS T_s products to study UHIs [Wang *et al.*, 2007b]. In this study, we further smoothed the time series of surface UHIs with a 15 day window to reduce the anisotropic effect of T_s on the surface UHIs [Lagouarde *et al.*, 2012; Lagouarde *et al.*, 2004].

3. Method

Forty-five stations in the central urban area were used as urban stations to study atmospheric and surface UHIs (Figure 1). To reveal the impact of urban impervious surfaces on the UHIs, we calculated the percentage of impervious surfaces within a circle around the stations using land cover data with a spatial resolution of 30 m derived from Landsat imagery data in 2013 [Li *et al.*, 2015; Wang *et al.*, 2015]. The amount of impervious surfaces can well represent the urbanization situation. For a circular area of 1 km², the percentage of impervious surfaces varied from 10% (i.e., the station in Olympic Park) to nearly 100% (i.e., the station in Tian'anmen Square) (Figure 3). This range narrowed as the circular area increased. For most stations, the percentage of impervious surfaces varied from 50% to 90% when the circular area was 5 km² (Figure 3). In this study, a 1 km² circle was selected because the MODIS T_s data used here have a spatial resolution of 1 km². By sorting the UHIs according to the percentage of impervious surfaces, we were able to clearly illustrate the impact of the impervious surfaces on the UHIs.

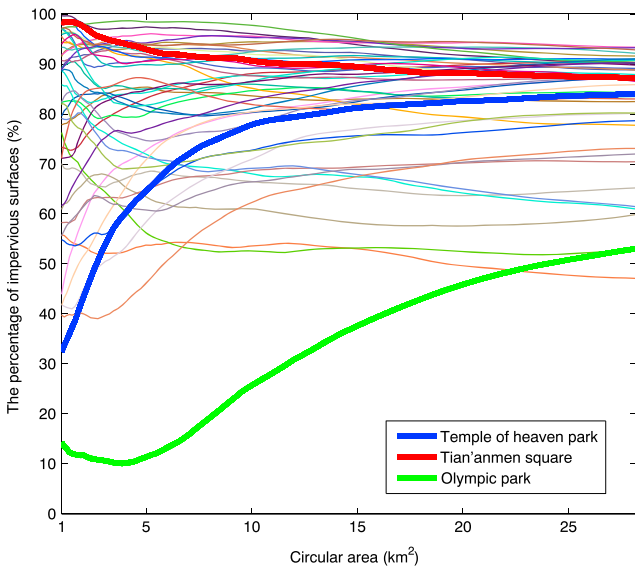


Figure 3. The dependence of the percentage of impervious surfaces of the 45 urban stations (as shown in Figure 1) on the scale of the calculation area. Each colored line represents an urban station. When the circular area used in the calculation was 1 km^2 , the percentage of impervious surfaces varied from 10% to nearly 100%. This range narrowed as the circular area used was increased. For most stations, the percentage of impervious surfaces varied from 50% to 90% when the calculation circular area was 5 km^2 . Three typical stations were shown in thick solid lines.

representative locations for the purpose of estimating UHI magnitude and Google Earth images around the stations are presented in Figure 2, and the locations of the four stations are presented in Figure 4. At the warning tower station, the AWS was located at a height of 16.6 m in a meteorological early warning tower on a street with tall buildings nearby. Its percentage of impervious surfaces was 91%. The Tian'anmen Square station was located in the vegetation belt of Tian'anmen Square with 98% of impervious surfaces, but distant from tall buildings. The station in China Meteorological Administration had 91% of impervious surfaces, and tall buildings were nearby. The Temple of Heaven Park station in the Temple of Heaven Park was surrounded by trees and had 32% of urban impervious surfaces, and the park was quite close to the center of the urban area. The percentage of impervious surfaces at the Temple of Heaven Park station increased with the circular area (Figure 3). Except for the warning tower station, the air temperature sensors were deployed 1.5 m above the surface, similar to a general weather station.

Here we divided urban surfaces into the following two types: vegetation and impervious surfaces. Impervious surfaces in this study include the canopy surfaces of buildings, roads, squares, and all other impervious constructions, which can well represent the urbanization situation, particularly in primary urban areas. We did not divide the surface into more detailed types. The three-dimensional urban morphology around the AWS may significantly affect the UHIs [Muller et al., 2013b; Stewart and Oke, 2012; Susaki et al., 2014]. However, we lack such data, and their impacts were not discussed quantitatively in this study. We selected four urban stations with strong variations in sky-view factors to qualitatively present their impacts (Figure 2).

For this study, we selected 4 out of the 45 urban stations to illustrate the diurnal and seasonal variations in their atmospheric and surface UHIs; fewer field sites in representative locations are preferable to more sites in unrepresentative locations [Stewart, 2011]. Photos of the stations and Google Earth images around the stations are presented in Figure 2, and the locations of the four stations are presented in Figure 4. At the warning tower station, the AWS was located at a height of 16.6 m in a meteorological early warning tower on a street with tall buildings nearby. Its percentage of impervious surfaces was 91%. The Tian'anmen Square station was located in the vegetation belt of Tian'anmen Square with 98% of impervious surfaces, but distant from tall buildings. The station in China Meteorological Administration had 91% of impervious surfaces, and tall buildings were nearby. The Temple of Heaven Park station in the Temple of Heaven Park was surrounded by trees and had 32% of urban impervious surfaces, and the park was quite close to the center of the urban area. The percentage of impervious surfaces at the Temple of Heaven Park station increased with the circular area (Figure 3). Except for the warning tower station, the air temperature sensors were deployed 1.5 m above the surface, similar to a general weather station.

The four stations were selected because they have strong contrast with their surrounding environments, i.e., vegetation coverage and sky-view factors. The normalized difference vegetation index (NDVI) of the four typical stations at the scale of 1.25 km derived from MODIS was shown in Figure 5, from

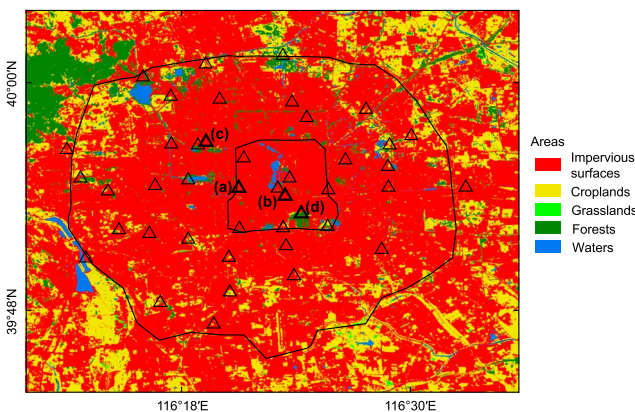


Figure 4. The magnified map of automatic weather stations. The second and fifth ring roads of Beijing City were shown in solid black lines. Land cover types in 30 m resolution was shown as background. The selected four urban stations were marked in the figure: (a) the warning tower station, (b) the Tian'anmen Square station, (c) the China Meteorological Administration station, and (d) the Temple of Heaven Park station, which is located in the Temple of Heaven Park.

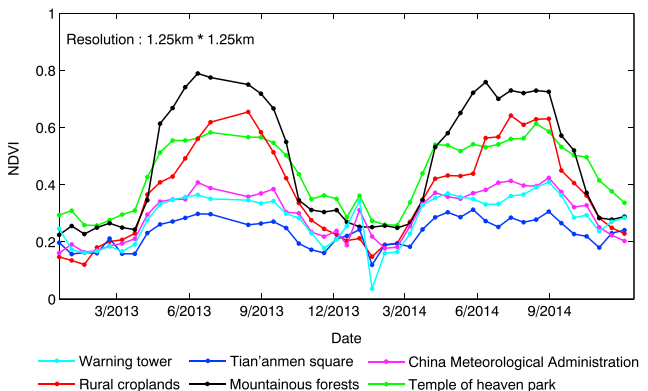


Figure 5. Time series of the normalized difference vegetation index (NDVI) derived from MODIS observations in the years 2013–2014.

buildings and has a low-sky-view factor (Figure 2). The warning tower station was selected to demonstrate the impact of the measurement height on atmospheric UHIs (Figure 2). The different combinations of the four stations enabled us to study the impacts of the openness of urban landforms around the stations and the air temperature measurement heights on the atmospheric and surface UHIs.



Figure 6. (a) Photos and Google Earth maps (b) during summer and (c) during winter of one typical rural cropland station (Gaoliying).

which one can identify obvious differences in green vegetation between these stations. The Temple of Heaven Park station is located near the center of the primary urban zones but with dense vegetation coverage (Figure 2). Therefore, its UHIs are weakly affected by urban structure but can be influenced by anthropogenic heat transported from nearby urban areas. Conversely, the Tian'anmen Square station and Chinese Meteorological Administration stations are strongly affected by urban buildings, although the former has a high-sky-view factor and the latter is surrounded by high buildings and has a low-sky-view factor (Figure 2). The warning tower station was selected to demonstrate the impact of the measurement height on atmospheric UHIs (Figure 2). The different combinations of the four stations enabled us to study the impacts of the openness of urban landforms around the stations and the air temperature measurement heights on the atmospheric and surface UHIs.

The rural cropland reference stations were selected based on the following three considerations: (1) The percentage of impervious surfaces around the stations had to be less than 30%, and the percentage of croplands had to be greater than 65%. (2) The surface elevation had to be less than 60 m above the mean sea level, which is nearly equal to the level of the urban stations. (3) The rural sites had to be outside major urban areas. Eleven stations met these requirements, as shown in Figure 1, and their data were averaged to represent a typical rural cropland station. Most crops in Beijing metropolitan grow in the summer and are harvested in October (Figures 5 and 6), such as wheat and corn.

Existing studies have reported that the selection of a rural reference station has a great impact on estimates of UHI intensity [Hawkins *et al.*, 2004; Sakakibara and Owa, 2005; Schwarz *et al.*, 2011; Wang *et al.*, 2007b]. We therefore also selected nine mountainous forest stations averaged as rural references and calculated their corresponding UHIs. The selection of mountainous forest stations was based on the following requirements: (1) The ratio of urban impervious surfaces had to be

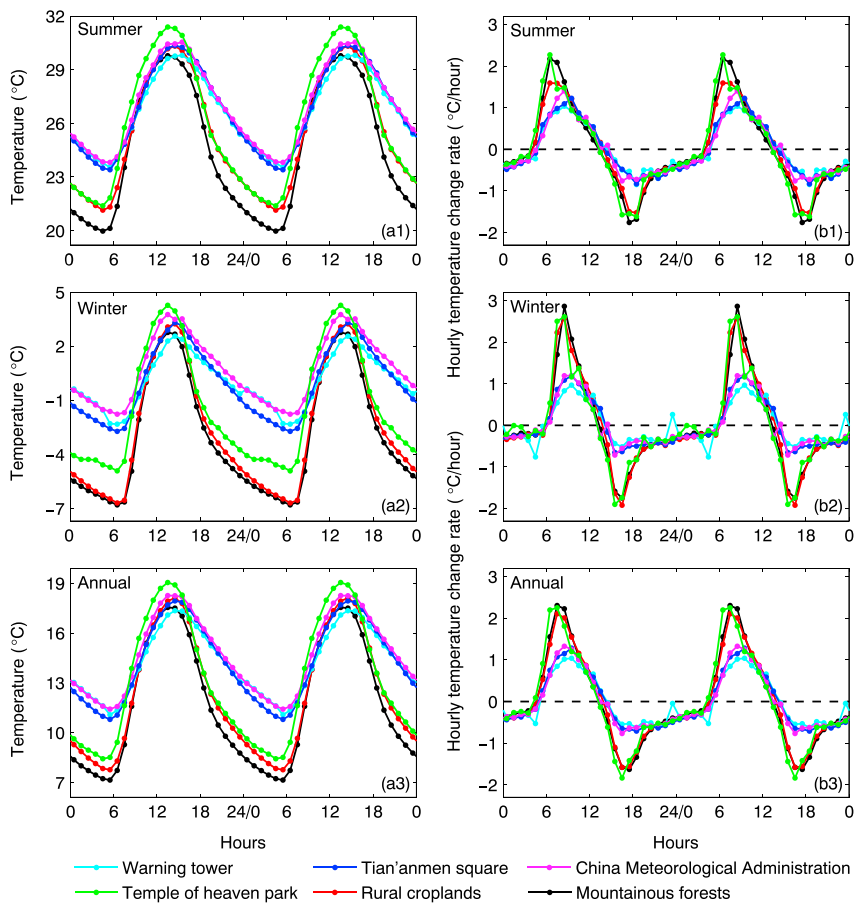


Figure 7. Time series of the (a1–a3) composite hourly air temperatures (T_a) and (b1–b3) hourly T_a change rates over six urban and rural stations. To reduce the impact of missing data and random measurement errors, we averaged the hourly air temperature (T_a) data within a given month to obtain hourly T_a values for each month, which were averaged to yield summer (June–August; Figure 7a1), winter (December–February; Figure 7a2), and annual (January–December; Figure 7a3) hourly T_a values. The data used here cover the period of 2013–2014.

less than 15%, and the ratio of forests had to be greater than 70%. (2) The surface elevation had to be less than 300 m above the mean sea level, in order to reduce the impact of surface elevation on T_a and T_s . (3) The rural sites had to be outside a major urban area. Because all of the selected mountainous forest stations were located in mountainous areas, their surface elevations are much higher than those of the urban stations. We corrected the temperatures (including T_a and T_s) by assuming that they decreased with height at a rate of 0.6°C per 100 m. This correction was empirical and may have a large uncertainty. Therefore, when comparing the UHIs referenced to mountainous forest stations with those referenced to rural cropland stations, we focused on their diurnal or seasonal changes rather than their absolute values.

To reduce the impact of the observational bias, we merged the data T_a or T_s of the 11 rural cropland stations together and obtained a rural cropland reference to study UHIs referenced to rural croplands. Similarly, we averaged T_a or T_s of the nine mountainous forest stations together after correcting for the impact of their surface elevations. When comparing the diurnal variability of UHIs, we first averaged the hourly T_a values in a given month to yield typical hourly T_a values for each station for each month; from these values, the seasonal and annual hourly averages shown in Figures 7–10 were calculated. When comparing seasonal variabilities (Figure 11), we used the method of linear interpolation to pair each available T_s datum with the AWS hourly T_a based on the satellite overpass time to reduce the impact of contemporaneous problems [Lowry, 1977].

The T_s data used in this study were retrieved from MODIS thermal infrared observations. Because the MODIS infrared detectors cannot penetrate clouds, the MODIS data are only available under clear-sky conditions. In

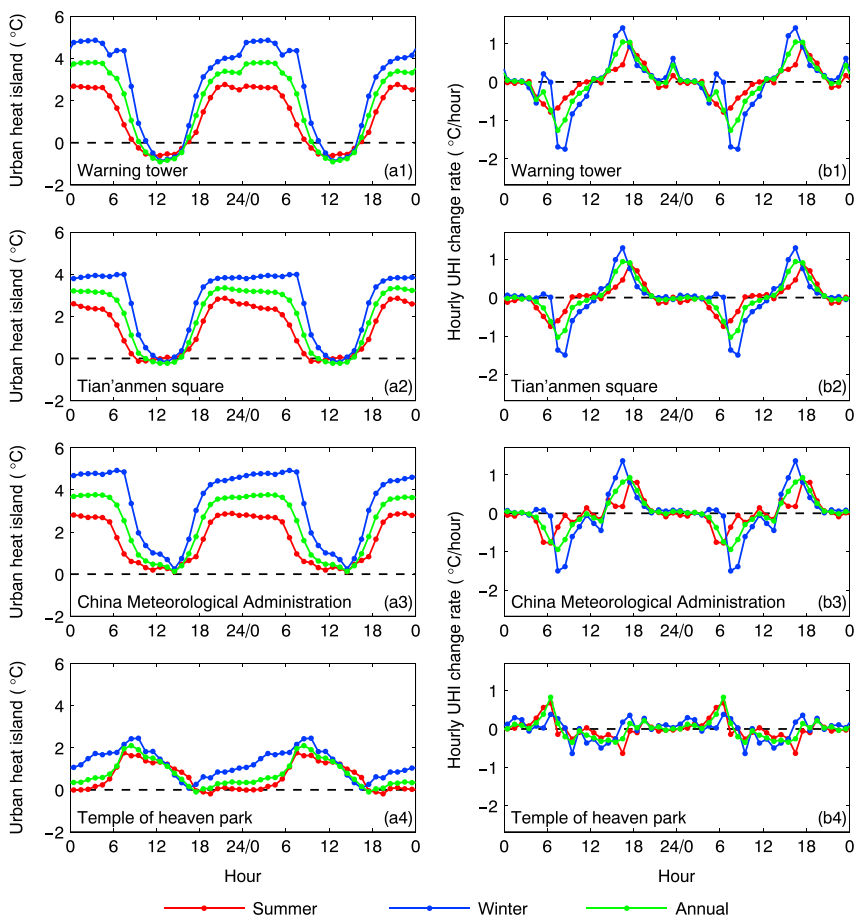


Figure 8. Time series of the (a1–a4) hourly atmospheric UHI data and (b1–b4) hourly atmospheric UHI change rates in terms of air temperature (T_a) at different urban stations, with rural cropland stations used as the rural references. The data processing method shown in Figure 7 was employed.

this study, we consider that it is a clear-sky condition if the MODIS T_s retrieval is available; otherwise, it is a cloudy condition. This definition of cloudy conditions is slightly different from a definition based on cloud fraction, i.e., cloud fraction being larger than 0.2 [An and Wang, 2015]. A recent study observed that these two definitions are quite consistent under most conditions [An and Wang, 2015]. We paired each available T_s datum (a maximum of four per day) with the AWS T_a (under clear-sky conditions) and T_{ac} (under cloudy conditions) based on the satellite overpass time at each station.

4. Results and Discussion

4.1. Diurnal and Seasonal Cycles of Atmospheric UHIs

Figure 7 depicts the summer (June–August), winter (December–February), and annual (entire year) diurnal cycles of T_a and their temporal evolution at different urban (including the urban park station) and rural stations in Beijing. The amplitudes of the T_a diurnal cycles differed significantly between the urban and rural stations. The most obvious difference occurred during nighttime. Urban areas were 3°C warmer during summer nights; this difference was twice as large in winter. Because the Temple of Heaven Park station was surrounded by trees (Figure 2), its nighttime T_a was similar to that of rural croplands in summer nighttime but was much greater in winter nighttime (Figure 7).

The T_a over mountainous forest stations was approximately the same as that of rural cropland stations during nighttime in winter, but it was much less over the mountainous forest stations than that over the rural cropland stations during summer nights. The absolute temperature value in mountainous forest stations may be

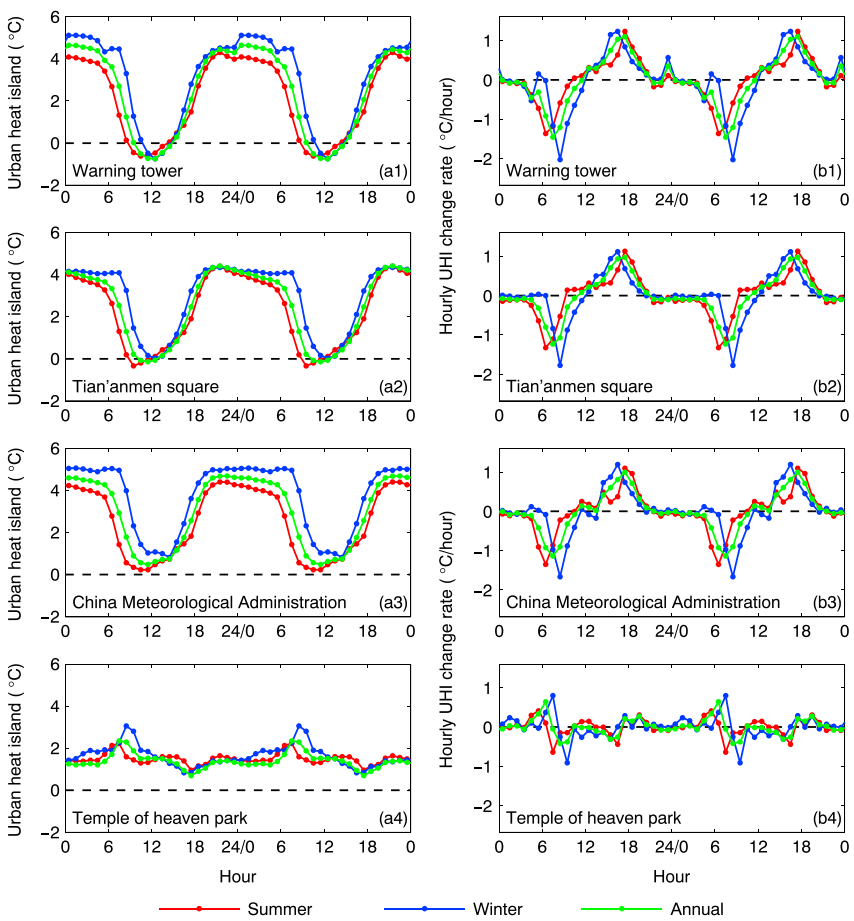


Figure 9. The same as Figure 8 but the mountainous forest stations were used as the rural references for the UHIs.

affected by the correction of assuming a constant long-term lapse rate of 0.6°C per 100 m. Therefore, we focused on the diurnal or seasonal changes of T_s and T_a rather than their absolute values in the analysis.

These differences in the diurnal cycles of T_a for the urban and rural stations lie in the heating and cooling rates of the different surface materials. After sunrise, T_a began to increase. However, the time at which T_a began to increase over the urban stations, except for the urban park station, was approximately 1 h later than that of the croplands and mountainous forest stations. The rate of increase over the rural croplands and mountainous forests was much greater than that over the typical urban stations, including the warning tower, Tian'anmen Square, and China Meteorological Administration stations. The rate of increase in T_a over the rural cropland and mountainous forest stations in winter was also greater than that in summer, and the highest rate of increase was approximately 3°C h^{-1} in winter and 2°C h^{-1} in summer. By contrast, for the urban stations, the rate of increase was approximately the same in summer and winter, with a maximum warming rate of 1°C h^{-1} .

Another significant difference between the urban and rural stations was that the maximum hourly temperature change rate at the rural stations occurred approximately 1–2 h earlier than that at the urban stations, except for the urban park station. In the afternoon, especially after 14:00, the rate of energy gain was less than the rate of energy loss, and T_a thus decreased at both the rural and urban stations. Similarly, the rate of decrease at the urban stations was much less than that at the rural stations. The maximum rate of decrease at the rural stations occurred approximately 1–2 h later than that at the urban stations, particularly in winter.

Figures 8a1–8a4 depict the atmospheric UHI over the selected four urban stations, with the rural cropland stations used as a rural reference. The nighttime atmospheric UHI was stronger and more stable than the daytime atmospheric UHI. The nighttime atmospheric UHI in winter was approximately 2°C greater than that in summer. The atmospheric UHI increased in winter nighttime, whereas it decreased in summer nighttime.

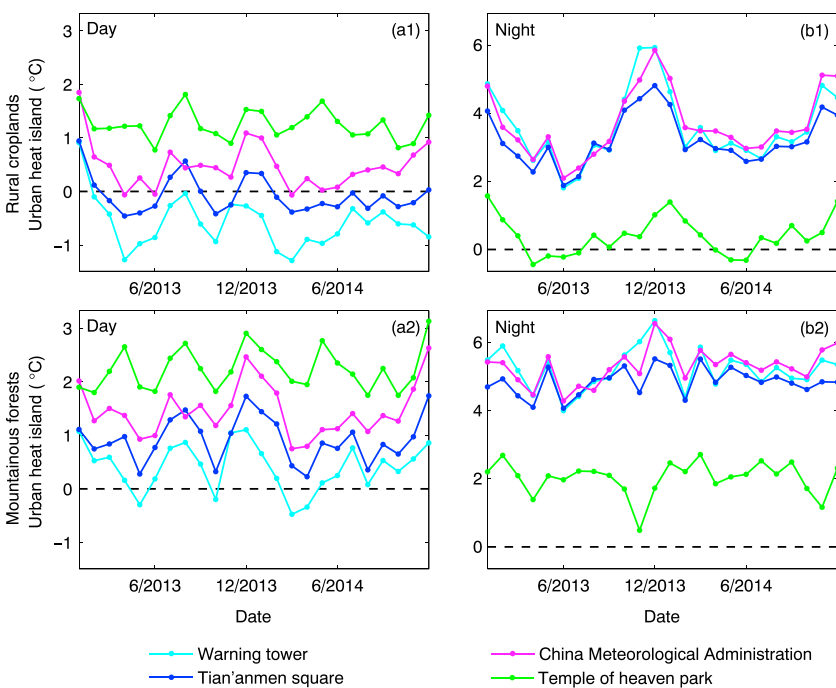


Figure 10. Time series of the monthly mean daytime (10:00 A.M. to 04:00 P.M.) and nighttime (10:00 P.M. to 04:00 A.M.) atmospheric UHIs according to air temperature (T_a) over different urban stations, with rural cropland stations and mountainous forest stations used as rural references, respectively.

These diurnal and seasonal variations were related to anthropogenic heat release caused by human activities, which is an important factor besides urban structure in determining atmospheric UHI.

It is acknowledged that human activities in urban areas emit a large amount of heat that can directly heat the air in and above the urban canopy. The heat can be released near the ground from motor traffic or from the roofs and walls of buildings. In general, anthropogenic heat release is greater in winter than in summer and is several times greater in the daytime than in the nighttime [*Jamarino et al.*, 2012; *Ichinose et al.*, 1999; *Sailor et al.*, 2015; *Tong et al.*, 2004]. In addition, heat is supplied all day in the urban area of Beijing during winter. Therefore, such changing anthropogenic heat release with time in different seasons caused the atmospheric UHI to be stronger at night, to increase with time during winter nights, and to decrease with time during summer nights (Figure 8).

The summer, winter, and annual mean values of nighttime atmospheric UHI at typical urban stations except for the park station were about 1.5°C, 2°C, and 1.8°C, respectively. Compared to the previous studies on atmospheric UHI over Beijing, the values were a little higher in our result. For example, *Yang et al.* [2013] analyzed the atmospheric UHIs at 64 meteorological stations and showed that the mean values of atmospheric UHI were 0.92°C and 1.65°C in summer and winter, respectively. *Y. Lu et al.* [2014] used meteorological observations over 20 stations in 2012 and showed that the annual mean atmospheric UHI was 1.3°C. This is because in this study we selected typical rural stations as rural reference (see section 4.2).

The atmospheric UHI at the Temple of Heaven Park station referenced to the rural cropland stations was stronger at daytime than at nighttime, which was quite different from the other three selected stations (Figure 8). The summer nighttime atmospheric UHI at the city park station was nearly zero, whereas the winter nighttime atmospheric UHI was approximately 1°C. We attributed the result to anthropogenic impacts. First, the Temple of Heaven Park station was set in the park which was quite close to the center of the urban area. Therefore, this station will inevitably be affected by anthropogenic impacts. Second, the station was not surrounded by buildings (Figure 2) and was not affected by the shadow effect of solar radiation during daytime and long-wave radiation reemitted from the nearby urban fabric material nighttime. Third, the diurnal cycle of T_a at the Temple of Heaven Park station is more similar to rural croplands and mountainous forests than other urban stations (Figure 7); i.e., T_a began to increase in the park approximately 1 h earlier than

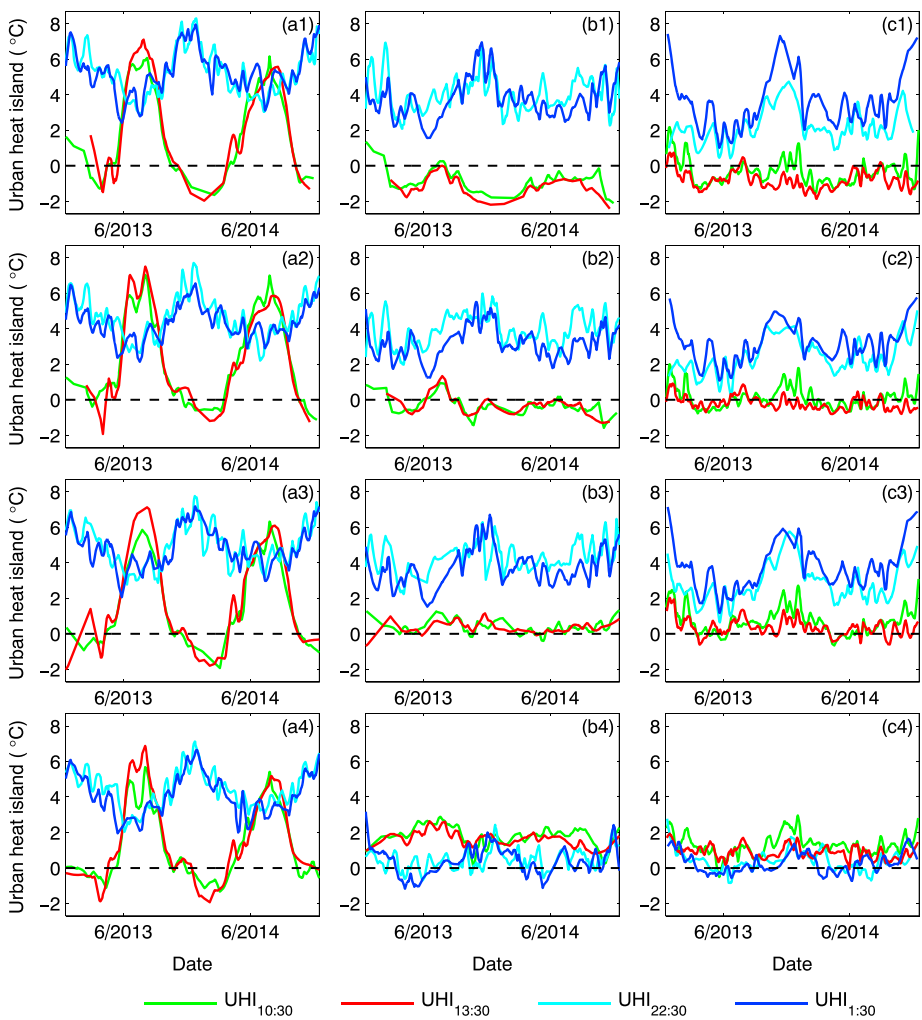


Figure 11. Time series of the (a1–a4) surface UHIs according to land surface temperature (T_s) at four time points during MODIS overpasses and (b1–b4) atmospheric UHIs according to air temperature (T_a) at the same times, with rural cropland stations used as the rural reference. For comparison, the (c1–c4) atmospheric UHIs according to T_a under cloudy conditions are also shown (T_{ac}). To reduce random errors and depict the seasonal UHI cycle, we smoothed the UHIs with a window of 15 days. Figures 11a1, 11b1, and 11c1 correspond to the UHIs of the warning tower; Figures 11a2, 11b2, and 11c2 correspond to the UHIs of Tian'anmen Square; Figures 11a3, 11b3, and 11c3 correspond to the UHIs of the China Meteorological Administration; Figures 11a4, 11b4, and 11c4 correspond to the UHIs of the Temple of Heaven Park.

that at the China Meteorological Administration station (Figure 7), which was surrounded by tall buildings. Therefore, the atmospheric UHI at the Temple of Heaven Park was likely to be dominated by anthropogenic heat which was stronger at daytime as well.

The temporal evolution of the atmospheric UHIs according to T_a at various urban stations is depicted in Figures 8b1–8b4. The atmospheric UHIs decreased after sunrise, and the rate of decrease reached a maximum 3 h later; however, the atmospheric UHIs continued to decrease during the morning. The atmospheric UHIs began to increase in the afternoon, and the maximum rate of increase was attained near sunset. Generally, the absolute values of hourly atmospheric UHI change rates during daytime in winter were greater than those during daytime in summer. However, the hourly atmospheric UHI change rates were asymmetric during daytime; the rates were higher in the late afternoon in summer and in the early morning in winter.

Figure 9 shows the time series of the atmospheric UHIs and their hourly change rates, with the mountainous forest stations used as rural references. They are similar to those shown in Figure 8, in which the rural cropland stations were used as rural references. However, there is an important difference between

Figures 8 and 9. The contrasts between the summer and winter nighttime atmospheric UHIs when using the mountainous forest stations as rural references were much less than those when using rural cropland stations as rural references. This seasonal difference occurred because compared to wintertime, the T_a over the mountainous forest stations in summer nighttime was much less than that of the rural cropland stations (Figure 7), resulting in higher summer nighttime atmospheric UHIs referenced to the mountainous forest stations.

Figure 10 illustrates the seasonal variations of the average daytime and nighttime atmospheric UHIs referenced to the rural cropland and mountainous forest stations. To demonstrate the contrast between the daytime and nighttime atmospheric UHIs, we used the averages from 10:00 A.M. to 04:00 P.M. and from 10:00 P.M. to 04:00 A.M. to represent the daytime and nighttime means, respectively. The nighttime atmospheric UHIs reached a minimum in summer and a maximum in winter, because anthropogenic heat release was stronger during winter nighttime, i.e., heating supply.

The nighttime atmospheric UHIs at the China Meteorological Administration station were greater than those at the Tian'anmen Square station due to its lower sky-view factor at the China Meteorological Administration station and its resulting higher reflections of long-wave radiation emission. During the day, the air above the urban canopy floor is unstable, and T_a decreases with height, which explains the negative daytime UHI in terms of T_a referenced to the warning tower station (Figure 8), keeping in mind that the T_a sensor at the warning tower station was high above the urban floor (Figure 2).

4.2. Comparisons of the Seasonal Cycles of the Atmospheric and Surface UHIs

Figures 11 and 12 compare the seasonal variations of the atmospheric and surface UHIs. For comparison, the atmospheric UHIs under cloudy conditions are also shown. To clearly compare the difference between the diurnal and seasonal cycles of the atmospheric and surface UHIs, only four types of urban stations are shown in Figures 11 and 12. Interstation comparisons and their statistical parameters are presented in Figures 14–17 and Tables 1–4. The contrasts of atmospheric UHIs between stations are much larger than those of surface UHIs (Figures 11 and 12). This is because the scale of T_a observations is much less than that of T_s , and station contrasts of the impervious surface ratio are higher at small scales (Figure 3).

Figure 11 shows that the nighttime atmospheric and surface UHIs referenced to the rural cropland stations exhibited similar seasonal cycles except for the Temple of Heaven Park station, but the nighttime surface UHIs were stronger than the atmospheric UHIs. However, the daytime surface and atmospheric UHIs differed substantially. The daytime surface UHIs exhibited a significant seasonal cycle, with a maximum value of +6°C in August and a negative value in winter. The daytime atmospheric UHIs exhibited a seasonal cycle that was similar to the daytime surface UHIs under clear-sky conditions but with a much smaller amplitude. The seasonal atmospheric UHI cycle under clear-sky conditions ($T_{a\text{c}}$; Figures 11b1–11b4) was not apparent under cloudy-sky conditions ($T_{a\text{c}}$; Figures 11c1–11c4).

Urbanization replaces vegetation (cropland or forests) with impervious surfaces. There are minimal amounts of water for evaporation and transpiration in urban areas, which leaves more energy transfer to the ground [Kato and Yamaguchi, 2007; Offerle *et al.*, 2005]. The soil heat flux can account for 50% of the total net radiation in the urban area of Beijing [Miao *et al.*, 2012], compared with approximately 10% for vegetated surfaces and up to 40% for bare soil [Cautenet *et al.*, 1986; Meyers and Hollinger, 2004]. The soil heat flux directly heats the surface and increases T_s . The urban-rural evapotranspiration contrast is more distinct in the summer because (1) the surface solar radiation is stronger in the summer, and the solar elevation is higher, which allows more energy to reach the urban canopy floor, and (2) the urban-rural vegetation coverage contrast is large in the summer (Figure 5). This factor explains the seasonal cycles of the daytime UHI in terms of T_s shown in Figures 11 and 12 and is also consistent with previous studies that revealed a significant correlation between the UHI in terms of T_s and the fraction of vegetation coverage in the city [Weng *et al.*, 2004; Zhou *et al.*, 2011].

The higher T_s in urban areas increases the instability of the air above the street floor in the summer and increases Q_H over urban areas, which directly heats the air above the surface and increases T_a . This phenomenon explains why the daytime UHI in terms of T_a exhibited a similar seasonal cycle to the daytime UHI in terms of T_s but with a much smaller amplitude (Figures 11 and 12). This seasonal cycle disappeared under cloudy conditions because the surface incident solar radiation was much weaker.

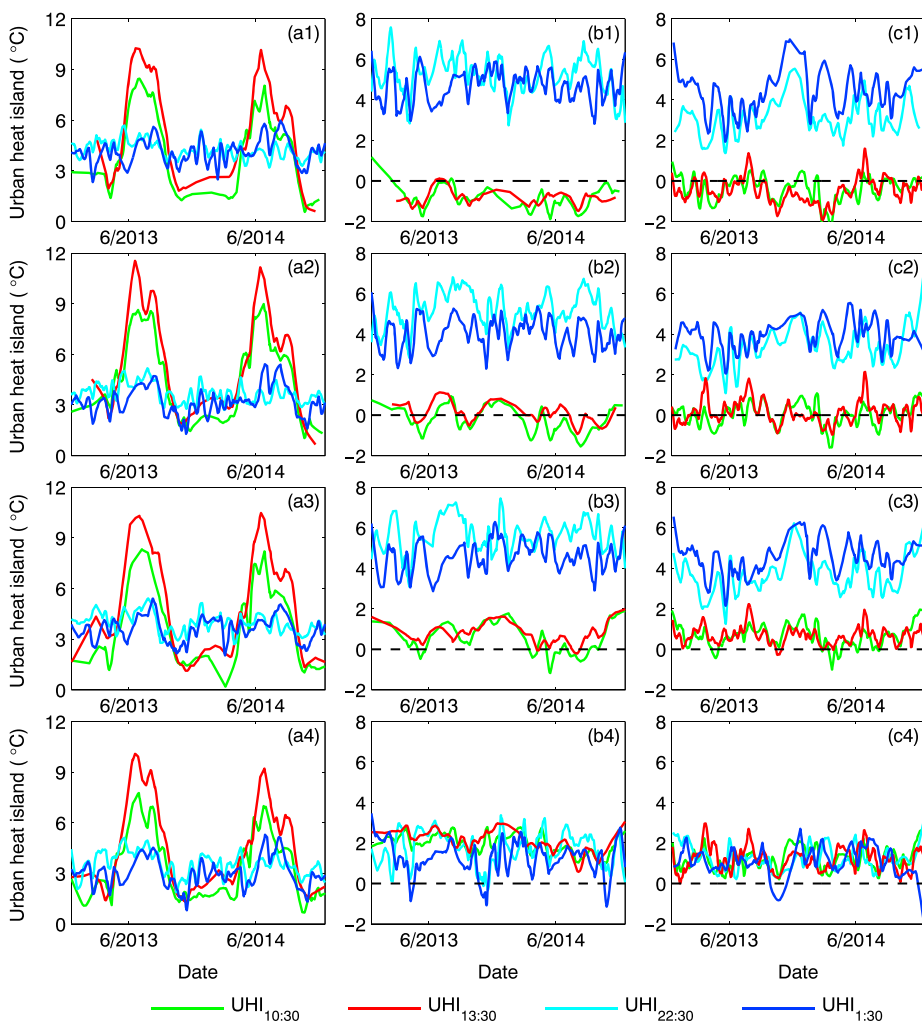


Figure 12. The same as Figure 11 but the mountainous forest stations were used as the rural references for the UHIs.

Table 1. Summer, Winter, and Annual Mean Surface UHIs in Terms of Land Surface Temperature (T_s) Under Clear-Sky Conditions, Atmospheric UHIs in Terms of Air Temperature (T_a) Under Clear-Sky Conditions, and Air Temperature Under Cloudy Conditions (T_{ac}) at Four Satellite Overpass Times During 1 Day (at Approximately 10:30, 13:30, 22:30, and 01:30, Beijing Time) (Units: °C)^a

Time	Season	Mean UHI (°C)			Slope ($10^{-2} \text{ }^{\circ}\text{C}/\%$)			R		
		T_s	T_a	T_{ac}	T_s	T_a	T_{ac}	T_s	T_a	T_{ac}
10:30	summer	4.19(6.52)	0.84(0.59)	0.23(0.47)	3.95(3.97)	-0.25(-0.20)	0.47(0.50)	0.74(0.74)	-0.08(-0.07)	0.26(0.29)
	winter	-0.27(1.86)	0.31(1.03)	1.17(0.68)	0.05(0.54)	-0.72(-0.27)	0.08(0.12)	0.02(0.24)	-0.24(-0.10)	0.04(0.06)
	annual	1.39(3.55)	0.46(0.66)	0.55(0.40)	1.97(2.16)	-0.42(-0.31)	0.18(0.18)	0.58(0.62)	-0.17(-0.12)	0.11(0.11)
13:30	summer	4.49(8.08)	0.80(0.94)	0.42(1.02)	3.38(3.57)	-0.21(-0.16)	0.46(0.55)	0.69(0.68)	-0.08(-0.06)	0.26(0.29)
	winter	-0.94(2.32)	-0.10(1.10)	0.49(0.38)	-0.40(0.69)	-1.23(-0.57)	-0.39(-0.23)	-0.13(0.19)	-0.38(-0.19)	-0.20(-0.12)
	annual	1.50(4.49)	0.32(0.83)	0.29(0.56)	2.02(2.29)	-0.52(-0.45)	0.01(0.08)	0.55(0.57)	-0.19(-0.17)	0.01(0.05)
22:30	summer	3.14(3.69)	2.58(4.20)	1.29(2.47)	0.37(0.45)	3.35(3.34)	2.22(2.17)	0.13(0.15)	0.70(0.70)	0.70(0.69)
	winter	5.20(2.78)	3.18(3.45)	2.37(2.94)	1.57(1.52)	3.87(3.84)	2.50(2.66)	0.27(0.26)	0.66(0.66)	0.61(0.61)
	annual	4.19(3.15)	2.80(3.82)	1.77(2.48)	0.85(0.85)	3.63(3.62)	2.28(2.34)	0.20(0.20)	0.71(0.71)	0.70(0.70)
01:30	summer	3.20(3.56)	1.70(3.00)	1.55(2.79)	0.71(0.69)	2.87(3.01)	2.48(2.46)	0.20(0.19)	0.74(0.73)	0.70(0.71)
	winter	5.04(2.56)	3.03(3.33)	3.22(2.96)	1.32(1.25)	3.38(3.19)	4.01(3.81)	0.23(0.22)	0.71(0.68)	0.65(0.64)
	annual	4.07(2.81)	2.41(3.07)	2.27(2.84)	0.77(0.74)	3.44(3.42)	3.19(3.15)	0.17(0.17)	0.73(0.72)	0.70(0.70)

^aThe mean UHIs referenced to rural cropland stations (mountainous forest stations) were averaged over the 45 urban stations. The UHI regression slopes as functions of the percentage of urban impervious surfaces and their correlation coefficients (R) are also listed (see Figures 14 and 15).

Table 2. The Square of Correlation Coefficients (R^2) Between Annual Mean Daytime Surface UHIs/Nighttime Atmospheric UHIs and the Percentage of Impervious Surfaces^a

Temperature	Time	Rural Croplands	Mountainous Forests
T_s	10:30	0.34	0.38
	13:30	0.31	0.33
T_a	22:30	0.50	0.50
	01:30	0.54	0.52
T_{ac}	22:30	0.49	0.50
	01:30	0.49	0.49

^aThe mean UHIs referenced to rural cropland stations (mountainous forest stations) were averaged over the 45 urban stations.

bare soils have lower thermal inertia than urban materials, and urban materials may receive less solar radiation because of strong atmospheric particulate pollution in urban areas [Jiang et al., 2010; Liu et al., 2003; Wang et al., 2003], which explains the negative daytime UHI in terms of T_s in April (Figure 11). Existing studies have shown that the impacts of urban-rural contrast of satellite-derived albedo and emissivity on surface UHIs over Beijing areas are negligible except for conditions after snow fall [Wang et al., 2007b]. After snow fall, the snow is removed in urban areas quickly but will remain for a relative long time in rural areas without disturbance.

Table 1 shows the mean values of atmospheric and surface UHIs over the 45 urban stations. The values of surface UHI were a little higher than those obtained in previous studies. Liu et al. [2016] showed that the mean value of daytime surface UHI from May 2013 to November 2013 was 2.3°C, whereas the contemporaneous daytime surface UHI in our study was about 3°C at the typical urban stations except for the park station. This result was obtained because we selected typical rural stations as rural references in this study (see section 4.2).

The annual mean of atmospheric UHI at 22:30 under clear-sky conditions was 1.03°C higher than that under cloudy-sky conditions over the 45 urban stations when referenced to rural cropland stations (see in Table 1). However, under clear-sky conditions, the atmospheric UHI decreased with time, i.e., the annual mean of atmospheric UHI at 22:30 was 0.39°C greater than that at 01:30 over the 45 urban stations when referenced to rural cropland stations. By contrast, under cloudy-sky conditions, the atmospheric UHI increased with time; i.e., the annual mean of atmospheric UHI at 22:30 was 0.5°C less than that at 01:30 under cloudy-sky conditions. Therefore, the annual mean of atmospheric UHI at 01:30 under clear-sky conditions was nearly equal to that under cloudy-sky conditions; i.e., the difference was 0.14°C when referenced to rural cropland stations. This phenomenon can be attributed to long-wave radiation. During nighttime, cloud reflection of long-wave radiation under cloudy-sky conditions enhanced the energy re-emission process. Therefore, atmospheric nighttime UHIs increase with time under cloudy-sky conditions and decrease with time under clear-sky conditions.

Figure 12 compares the seasonal variations in the atmospheric and surface UHIs referenced to mountainous forest stations. The seasonal contrasts in the nighttime UHIs referenced to mountainous forest stations were much less than those referenced to rural cropland stations, which exhibited significant seasonal cycles; i.e., the contrasts were greater in winter. We also observed that the summer nighttime surface UHIs at 01:30 referenced to mountainous forest stations were only 0.36°C greater than those referenced to rural cropland stations in Table 1. However, the mean winter nighttime surface UHIs at 01:30 referenced to mountainous

In winter and spring, rural croplands consist of dry bare soils without vegetation coverage (Figure 6), and the contrast in evapotranspiration between urban and rural areas is nearly zero. On the contrary, the green-up date in Beijing urban areas may be approximately 24 days earlier than that of the nearby rural areas [Wang et al., 2014; Zhou et al., 2016]. In early April, vegetation is already growing in Beijing urban area, whereas rural croplands remain covered by bare soil (Figure 6c). Dry bare soils have lower thermal inertia than urban materials, and urban materials may receive less solar radiation because of strong atmospheric particulate pollution in urban areas [Jiang et al., 2010; Liu et al., 2003; Wang et al., 2003], which explains the negative daytime UHI in terms of T_s in April (Figure 11). Existing studies have shown that the impacts of urban-rural contrast of satellite-derived albedo and emissivity on surface UHIs over Beijing areas are negligible except for conditions after snow fall [Wang et al., 2007b]. After snow fall, the snow is removed in urban areas quickly but will remain for a relative long time in rural areas without disturbance.

Table 3. The Slopes and Correlation Coefficients (R) of the Best Fitting Lines of the Surface Urban Heat Island (UHI) at 13:30 in Summer and Nighttime Atmospheric UHIs at 22:30 Shown in Figure 16

		UHI of T_s in Summer at 13:30		Slope (°C/°C)	
		<i>R</i>		Rural Croplands	Mountainous Forests
Season		Rural Croplands	Mountainous Forests	Rural Croplands	Mountainous Forests
UHI of T_a at 22:30	summer	0.37	0.33	0.56	0.47
	winter	0.38	0.36	0.74	0.61
	annual	0.41	0.38	0.66	0.56

Table 4. The Correlation Coefficients (R) Between the Summer and Winter UHIs Derived From T_s , T_a , and T_{ac} ^a

UHI		R Between Summer and Winter UHIs		Slope	
Temperature	Time	Rural Croplands	Mountainous Forests	Rural Croplands	Mountainous Forest
T_s	10:30	0.15	0.40	0.28	0.94
	13:30	0.08	0.41	0.13	0.60
	22:30	0.94	0.96	0.46	0.49
	01:30	0.91	0.94	0.56	0.58
T_a	10:30	0.41	0.41	0.40	0.42
	13:30	0.57	0.52	0.45	0.43
	22:30	0.90	0.91	0.73	0.74
	01:30	0.89	0.90	0.73	0.80
T_{ac}	10:30	0.46	0.50	0.41	0.45
	13:30	0.41	0.43	0.35	0.39
	22:30	0.82	0.81	0.63	0.59
	01:30	0.88	0.88	0.51	0.51

^aThe slope of the best fitting lines of the summer and winter UHIs derived from T_s , T_a , and T_{ac} . The corresponding scatterplots were shown in Figure 17. The high correlation between the winter and summer UHIs indicates that they were determined by similar factors in winter and summer. Similarly, if the coefficient is low (e.g., the surface UHIs referenced to rural cropland stations in daytime), they were dominated by different factors.

forest stations was 2.48°C less than that referenced to rural cropland stations (Table 1). This difference occurred because mountainous forests have a smaller long-wave cooling efficiency than rural croplands during winter when rural croplands are nearly bare soil (Figure 6), which is related to the multiple reflections of long-wave radiation.

Figure 13 explains these differences in seasonal variations of surface UHIs referenced to rural cropland and mountainous forest stations. The most important differences in T_s over mountainous forest and rural cropland stations is that T_s over mountainous forests is much lower than that over rural croplands during spring and summer daytime; i.e., the values of their difference after the elevation effect correction were 3.1°C and 3.8°C at 10:30 and 13:30, respectively.

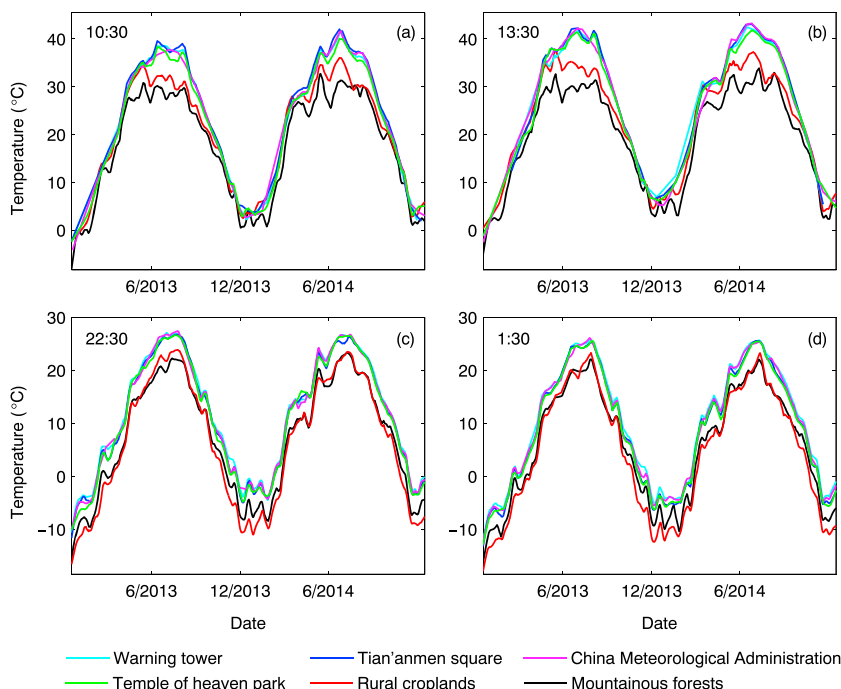


Figure 13. Time series of the 15 day smoothed land surface temperature (T_s) over six urban and rural stations at four MODIS overpass times: (a) 10:30, (b) 13:30, (c) 22:30, and (d) 01:30. The T_s data are only available under clear-sky conditions.

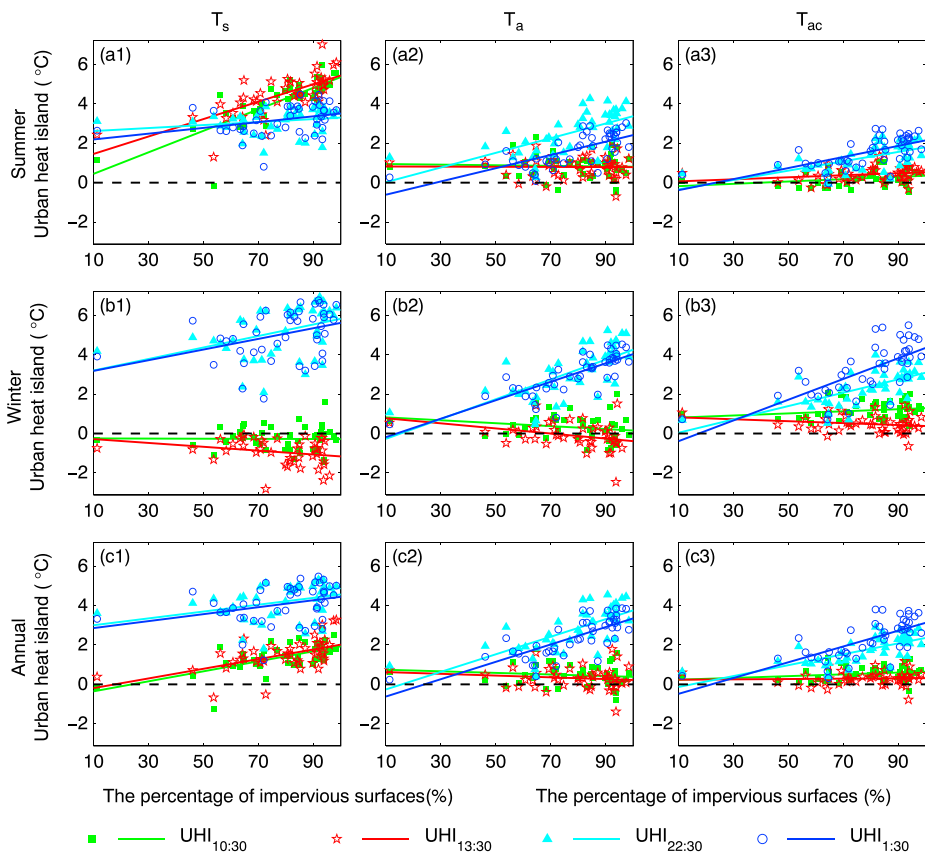


Figure 14. (a1, b1, and c1) The surface UHIs derived from land surface temperature (T_s) at four MODIS satellite overpass times and (a2, b2, and c2) atmospheric UHIs derived from air temperature (T_a) at the same times as a function of the percentage of impervious surfaces around the urban stations. T_s was available only under clear-sky conditions. For comparison, (a3, b3, and c3) the atmospheric UHIs derived from T_a under cloudy conditions are also shown (T_{ac}). The summer (Figures 14a1–14a3), winter (Figures 14b1–14b3), and annual (Figures 14c1–14c3) mean UHIs are shown. Each point represents a station in the panel, and all 45 urban stations are used here. The rural cropland stations were used as the rural references. The best fitting lines are shown in the figures, and the statistics of the UHIs are presented in Table 1.

Another important difference in T_s over rural croplands and mountainous forests is that T_s over mountainous forests is much higher than that over rural croplands during nighttime in winter (Figure 13), which explains why the winter nighttime surface UHIs referenced to mountainous forest stations are much less than those referenced to rural cropland stations. This results in negligible seasonal variation of surface UHI referenced to mountainous forest stations (Figure 12).

4.3. Interstation Variability in the Atmospheric and Surface UHIs

This section compares the atmospheric and surface UHIs at the 45 urban stations and shows their dependence on the percentage of impervious surfaces of the urban stations. Figure 14 presents scatterplots of annual mean atmospheric and surface UHIs referenced to rural cropland stations as a function of the percentage of impervious surfaces around the urban stations. The annual nighttime atmospheric UHIs were closely related to the percentage of impervious surfaces around the urban stations. For example, their correlation coefficient was 0.73 at 01:30 when referenced to rural croplands, as seen in Table 1, and the square of their correlation coefficient is shown in Table 2.

From the R^2 values, we found that the percentage of impervious surfaces could explain 49%–54% of the variability of atmospheric UHIs. This phenomenon can be partially explained by anthropogenic impacts, which was stronger at nighttime. Most anthropogenic heat is directly released into the air and has a stronger impact on atmospheric UHIs than surface UHIs. The relation between the annual mean nighttime atmospheric UHIs at 22:30 and the percentage of impervious surfaces was nearly identical to that of the UHIs at

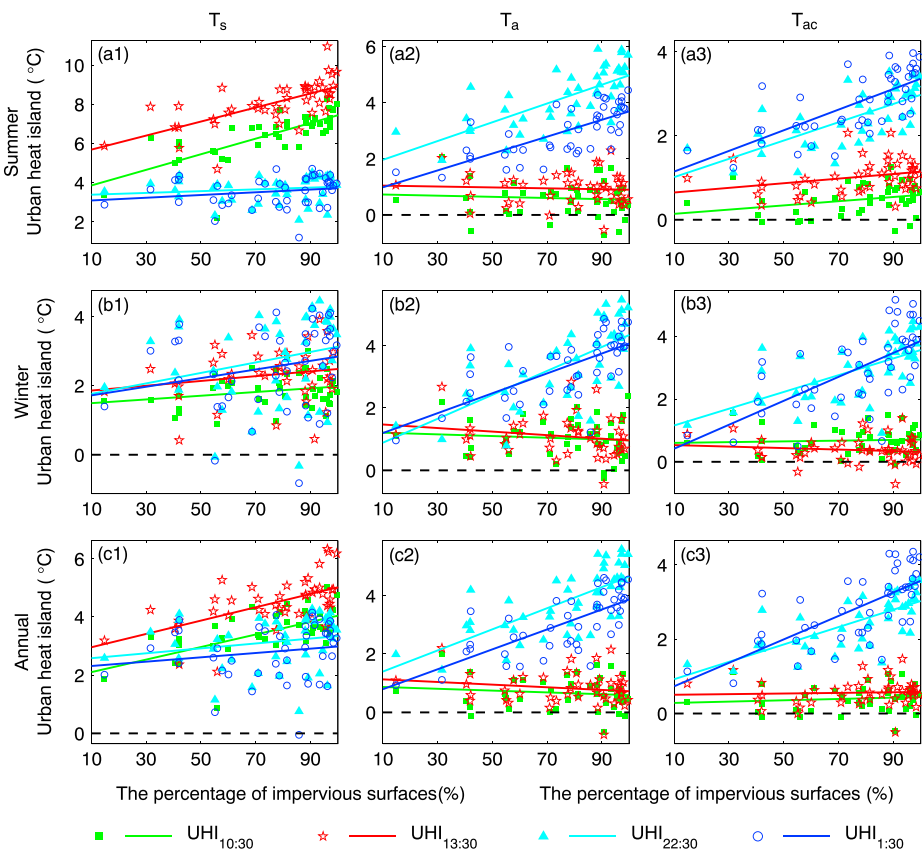


Figure 15. The same as Figure 14 but the mountainous forest stations were used as the rural references for the UHIs.

01:30 under clear-sky conditions. However, the slope for the UHI at 22:30 was much less than that at 01:30 under cloudy-sky conditions. The annual mean daytime atmospheric UHI under clear-sky conditions was only slightly negatively correlated with the percentage of impervious surfaces. Under cloudy conditions, the relationship varied from weak and negative in winter to weak and positive in summer.

The summer daytime surface UHI was closely related to the percentage of impervious surfaces around the urban stations. For example, their correlation coefficient was 0.74 at 10:30 when referenced to rural croplands, as seen in Table 1, and the square of their correlation coefficient was shown in Table 2. However, this dependence disappeared for the winter daytime surface UHI. From the *R*-square value, we found that the percentage of impervious surfaces could explain 31%–38% of the interstation variability of annual-mean surface UHIs.

Furthermore, the nighttime surface UHI was apparently uncorrelated with the percentage of impervious surfaces around the urban stations. We tried to correlate the nighttime surface UHIs with the percentage of impervious surfaces calculated by using different circular areas, and the results did not change significantly (Figures S1 and S2 in the supporting information). Figure 15 shows that the dependence of the UHIs referenced to mountainous forest stations on the percentage of impervious surfaces was similar to that of the UHIs referenced to rural cropland stations.

The anthropogenic heat is directly released to the air, which is difficult to transfer to the land surface, particularly at night when the surface layer is controlled by temperature inversion. This phenomenon may explain why the percentage of impervious surfaces dominates interstation variability of nighttime atmospheric UHIs but is nearly uncorrelated with nighttime surface UHIs. The percentage of impervious surfaces could not reflect the three-dimensional structure of the urban area. However, we do not have urban structure information, which requires further studies using lidar data [Susaki *et al.*, 2014; Yan *et al.*, 2015].

Figure 16 showed the correlation between surface UHIs at 13:30 in summer and the nighttime atmospheric UHIs at 22:30, and the correlation coefficients between them were calculated in Table 3. The stations partially

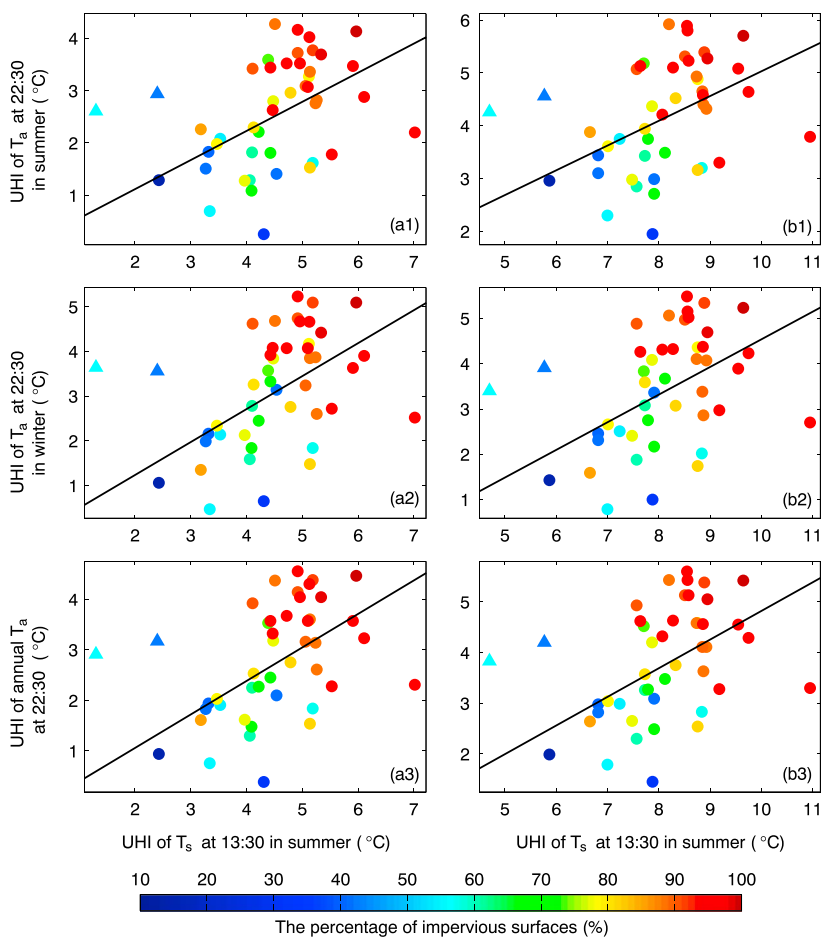


Figure 16. Scatterplots of surface UHIs at midday (13:30) in summer as a function of the nighttime atmospheric UHIs referenced (a1–a3) to the rural cropland station and (b1–b3) to the mountainous forest stations at 22:30. Each point represents a station, and the color shows the percentage of impervious surfaces of the urban stations. The best fitting lines are shown in the figures, and the statistics regarding the UHIs are presented in Table 3. The UHIs referenced to the rural cropland stations were used here. The stations partially surrounded by bodies of water (lakes and rivers) were indicated by triangles.

surrounded by bodies of water (lakes and rivers) had lower T_s in daytime and higher T_a in nighttime; therefore, they had lower daytime surface UHIs and higher nighttime atmospheric UHIs. The nighttime atmospheric UHI was higher when the percentage of impervious surfaces was high (Figure 16).

Although the summer daytime surface and nighttime atmospheric UHIs were both closely related to the percentage of impervious surfaces, the correlation coefficients reached 0.7 (see in Table 1), and their correlation coefficients were low, varying from 0.33 to 0.41 (see in Table 3). This is because daytime surface UHI and nighttime atmospheric UHI are determined by different physical process. Daytime surface UHI is determined by the reduction of the evaporative cooling effect due to the high percentage of impervious surfaces whereas nighttime atmospheric UHI is determined by anthropogenic heat release from urban areas.

Figure 17 showed the scatterplots of the summer UHIs as a function of the winter ones at the four satellite overpass times. The correlation coefficients between the winter and summer UHIs are calculated in Table 4. Figures 17a1 and 17a2 indicated that the summer nighttime surface UHI was closely related to the winter time surface UHI, and their correlation coefficients were 0.91–0.96 (see Table 4), indicating that their UHI spatial patterns are similar and they are determined by the same factors in winter and summer (i.e., the multiple reflections of long-wave radiation emitted by the materials of urban structures). The correlations between the summer and winter nighttime atmospheric UHIs were the second highest under both clear and cloudy conditions, demonstrating that they are also determined by similar factors (Figure 16 and

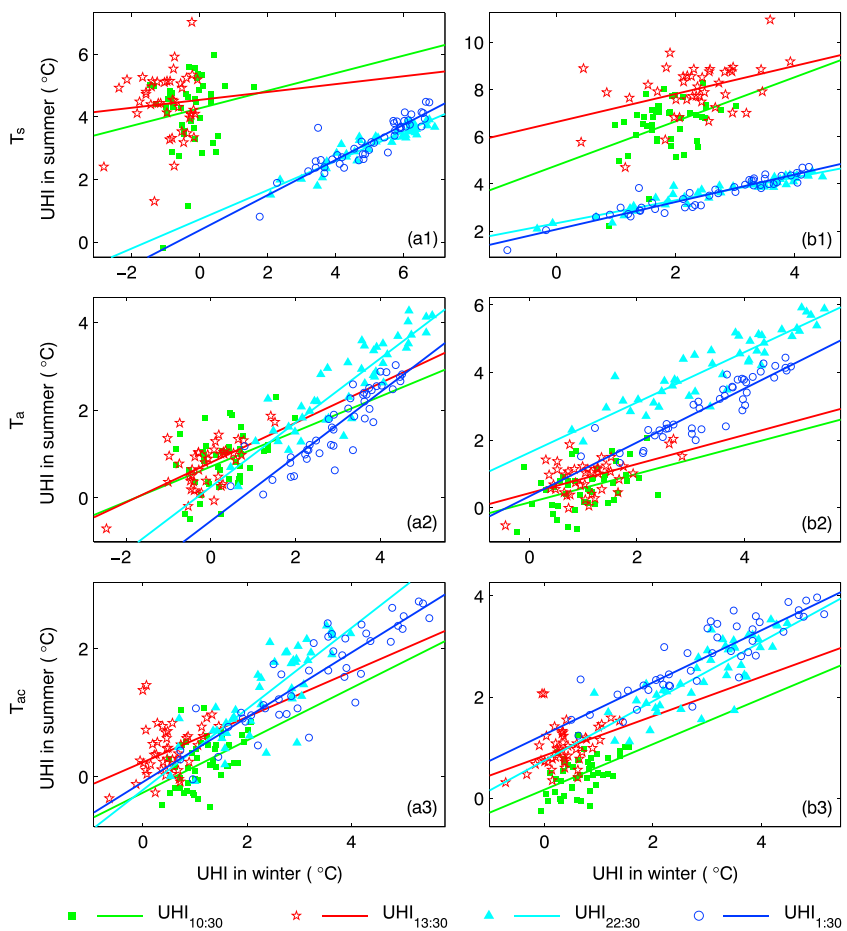


Figure 17. Scatterplots of the summer UHIs as a function of the winter ones at the four satellite overpass times: (a1) surface UHIs referenced to rural cropland stations, (b1) surface UHIs referenced to mountainous forest stations, (a2) atmospheric UHIs referenced to rural cropland stations under clear-sky conditions, (b2) atmospheric UHIs referenced to mountainous forest stations under clear-sky conditions, (a3) atmospheric UHIs referenced to rural cropland stations under cloudy conditions, and (b3) atmospheric UHIs referenced to mountainous forest stations under cloudy conditions. Each point represents a station. The best fitting lines are shown in the figures, and the statistics regarding the UHIs are presented in Table 4.

Table 4). However, the correlations between the summer and winter daytime UHIs were much less, particularly for surface UHIs (Figure 17 and Table 4).

5. Conclusions

In this study, we compared the diurnal and seasonal cycles of atmospheric and surface UHIs over the Beijing metropolitan area using hourly T_a data collected at Beijing metropolitan AWS network stations in the years of 2013–2014 and from four daily MODIS satellite T_s retrievals. From these comparisons, the determining factors of the surface and atmospheric UHIs were inferred.

Urbanization alters the land cover and land use types, thereby changing the radiative and turbulent processes of land-atmosphere system in several ways. First, urban structures reduce the amount of solar radiation that reaches the urban canopy floor during daytime, and part of the solar radiation is stored and re-emitted later as long-wave radiation. During nighttime, the multiple reflections of long-wave radiation emitted by the materials of urban structures reduce the long-wave cooling efficiency in urban areas. Second, human activities in urban areas release a large amount of heat, which can directly heat the air. Third, urbanization replaces vegetation (croplands or forests) with impervious surfaces and substantially reduces evapotranspiration and its cooling effect during daytime [Wang and Dickinson, 2012; Wang et al., 2010a, 2010b].

These three factors work together but differently for atmospheric and surface UHIs. The multiple reflections between urban materials make long-wave radiative cooling less efficient. This phenomenon is the major reason for the nighttime surface UHI. The reduction of the cooling effect of evapotranspiration due to more impervious surfaces in urban areas dominates the daytime surface UHIs. Atmospheric UHIs are primarily controlled by the energy stored in urban materials and its release during nighttime, in addition to anthropogenic heat release. The stronger anthropogenic heat release in winter causes atmospheric UHIs to increase with time during winter nights and decrease with time during summer nights. Similarly, cloud reflection of long-wave radiation under cloudy-sky conditions enhances the energy re-emission process during nighttime, which explains why the atmospheric nighttime UHIs increased with time under cloudy-sky conditions and decreased with time under clear-sky conditions.

The seasonal cycles of the nighttime atmospheric and surface UHIs depended on the selection of rural reference stations. The nighttime atmospheric and surface UHIs referenced to the rural cropland station exhibited significant seasonal cycles; i.e., they were higher in winter. However, the seasonal contrast in the UHIs referenced to the mountainous forest stations was almost zero. This result was obtained because mountainous forests had higher nighttime T_s values than rural croplands in winter and lower nighttime T_a than rural croplands in summer.

The percentage of impervious surfaces calculated from land cover and land use data sets has been widely used in studies of atmospheric and surface UHIs. This study found that this percentage can be used to well quantify the spatial variabilities of vegetation coverage and evapotranspiration, and it can also be understood as an index of the spatial variability in anthropogenic heat release. Therefore, the percentage of impervious surfaces explains 49%–54% of the interstation variabilities in nighttime atmospheric UHIs and 31%–38% of that in daytime surface UHIs. However, the percentage of impervious surfaces cannot reflect the three-dimensional structure of urban fabric structures and therefore is nearly uncorrelated with the interstation variability in the nighttime surface UHIs. Therefore, the impact of urban three-dimensional structures on surface UHIs in terms of T_s should be further studied, i.e., using lidar data [Susaki *et al.*, 2014; Yan *et al.*, 2015].

UHIs are arguably “well described but rather poorly understood” [Arnfield, 2003; Oke, 1982]. This paper provides a case study in Beijing using hourly T_a observations and satellite T_s retrievals. Additional studies are required at other locations and with more detailed observations, including three-dimensional observations of urban canopy boundary layers [Chapman *et al.*, 2015; Mestayer *et al.*, 2005; Tan *et al.*, 2015; Wood *et al.*, 2013], which will advance our understanding of UHIs and their causes.

Acknowledgments

This study was funded by the National Natural Science Foundation of China (41525018 and 41505134). The land cover type data at 30 m resolution in 2013 shown in Figure 1 were provided by Peng Gong from Tsinghua University. Qihao Weng from Indiana State University provided insightful comments. The Beijing Metropolitan Automatic Weather Station Network data were obtained from the Chinese Meteorological Administration. The MODIS satellite land surface temperature products were downloaded from <https://lpdaac.usgs.gov/>. The NDVI products derived from MODIS were downloaded from <http://daac.ornl.gov/MODIS/>.

References

- An, N., and K. Wang (2015), A comparison of MODIS-derived cloud fraction with surface observations at Five SURFRAD sites, *J. Appl. Meteorol. Climatol.*, 54(5), 1009–1020, doi:10.1175/jamc-d-14-0206.1.
- Arnfield, A. J. (2003), Two decades of urban climate research: A review of turbulence, exchanges of energy and water, and the urban heat island, *Int. J. Climatol.*, 23(1), 1–26, doi:10.1002/joc.859.
- Azevedo, J., L. Chapman, and C. Muller (2016), Quantifying the daytime and night-time urban heat Island in Birmingham, UK: A comparison of satellite derived land surface temperature and high resolution air temperature observations, *Remote Sens.*, 8(2), 153, doi:10.3390/rs8020153.
- Bassett, R., X. Cai, L. Chapman, C. Heaviside, J. E. Thorne, C. L. Muller, D. T. Young, and E. L. Warren (2016), Observations of urban heat island advection from a high-density monitoring network, *Q. J. R. Meteorol. Soc.*, 142, 2434–2441, doi:10.1002/qj.2836.
- Cautenet, G., M. Legrand, Y. Coulibaly, and C. Boutin (1986), Computation of ground surface conduction heat flux by Fourier analysis of surface temperature, *J. Climate Appl. Meteorol.*, 25(3), 277–283, doi:10.1175/1520-0450(1986)025<0277:cogsch>2.0.co;2.
- Chapman, L., J. A. Azevedo, and T. Prieto-Lopez (2013), Urban heat and critical infrastructure networks: A viewpoint, *Urban Clim.*, 3, 7–12, doi:10.1016/j.uclim.2013.04.001.
- Chapman, L., C. L. Muller, D. T. Young, E. L. Warren, C. S. B. Grimmond, X.-M. Cai, and E. J. S. Ferranti (2015), The Birmingham urban climate laboratory: An open meteorological test bed and challenges of the Smart City, *Bull. Am. Meteorol. Soc.*, 96(9), 1545–1560, doi:10.1175/bams-d-13-00193.1.
- Chen, A. L., L. Yao, R. H. Sun, and L. D. Chen (2014), How many metrics are required to identify the effects of the landscape pattern on land surface temperature?, *Ecol. Indic.*, 45, 424–433, doi:10.1016/j.ecolind.2014.05.002.
- Chen, H., Y. Zhang, M. Yu, W. Hua, S. Sun, X. Li, and C. Gao (2015), Large-scale urbanization effects on eastern Asian summer monsoon circulation and climate, *Clim. Dyn.*, 47, 117–136, doi:10.1007/s00382-015-2827-3.
- Choi, Y. Y., M. S. Suh, and K. H. Park (2014), Assessment of surface urban heat islands over three megacities in East Asia using land surface temperature data retrieved from COMS, *Remote Sens.*, 6(6), 5852–5867, doi:10.3390/rs6065852.
- Chow, W. T. L., D. Brennan, and A. J. Brazel (2012), Urban heat island research in Phoenix, Arizona: Theoretical contributions and policy applications, *Bull. Am. Meteorol. Soc.*, 93(4), 517–530, doi:10.1175/bams-d-11-00011.1.
- Clinton, N., and P. Gong (2013), MODIS detected surface urban heat islands and sinks: Global locations and controls, *Remote Sens. Environ.*, 134, 294–304, doi:10.1016/j.rse.2013.03.008.

- Dou, Y., Y. Qu, S. Tao, and B. Hu (2008), The application of quality control procedures for real time data from automatic weather stations, *Meteorol. Mon.*, 34(8), 77–81.
- Feng, H. H., H. P. Liu, and L. C. Wu (2014), Monitoring the relationship between the land surface temperature change and urban growth in Beijing, China, *IEEE J. Sel. Top. Appl. Earth Observ. Remote Sens.*, 7(10), 4010–4019, doi:10.1109/jstars.2013.2264718.
- Gallo, K. P., J. D. Tarpley, A. L. McNab, and T. R. Karl (1995), Assessment of urban heat islands—A satellite perspective, *Atmos. Res.*, 37(1–3), 37–43, doi:10.1016/0169-8095(94)00066-m.
- Gluch, R., D. A. Quattrochi, and J. C. Luval (2006), A multi-scale approach to urban thermal analysis, *Remote Sens. Environ.*, 104(2), 123–132, doi:10.1016/j.rse.2006.01.025.
- Hawkins, T. W., A. J. Brazel, W. L. Stefanov, W. Bigler, and E. M. Saffell (2004), The role of rural variability in urban heat island determination for Phoenix, Arizona, *J. Appl. Meteorol.*, 43(3), 476–486, doi:10.1175/1520-0450(2004)043<0476:trorvi>2.0.co;2.
- Howard, L. (1833), *The Climate of London*, pp. 348, Harvey and Darton, London.
- Hu, X.-M., M. Xue, P. M. Klein, B. G. Illston, and S. Chen (2016), Analysis of urban effects in Oklahoma City using a dense surface observing network, *J. Appl. Meteorol. Climatol.*, 55(3), 723–741, doi:10.1175/jamc-d-15-0206.1.
- Iamarino, M., S. Beavers, and C. S. B. Grimmond (2012), High-resolution (space, time) anthropogenic heat emissions: London 1970–2025, *Int. J. Climatol.*, 32(11), 1754–1767, doi:10.1002/joc.2390.
- Ichinose, T., K. Shimodono, and K. Hanaki (1999), Impact of anthropogenic heat on urban climate in Tokyo, *Atmos. Environ.*, 33(24–25), 3897–3909, doi:10.1016/s1352-2310(99)00132-6.
- Imhoff, M. L., P. Zhang, R. E. Wolfe, and L. Bounoua (2010), Remote sensing of the urban heat island effect across biomes in the continental USA, *Remote Sens. Environ.*, 114(3), 504–513, doi:10.1016/j.rse.2009.10.008.
- Jiang, Y.-h., Q. Wang, H. Zhang, Z. Wang, and B. Hu (2010), Radiation characteristics of urban boundary layer measured on the meteorological tower in Beijing, *Plateau Meteorol.*, 29(4), 919–928.
- Jin, M., and J. M. Shepherd (2005), Inclusion of urban landscape in a climate model - How can satellite data help?, *Bull. Am. Meteorol. Soc.*, 86(5), 681–689, doi:10.1175/bams-86-5-681.
- Jones, P. D., and D. H. Lister (2009), The urban heat island in Central London and urban-related warming trends in Central London since 1900, *Weather*, 64(12), 323–327, doi:10.1002/wea.432.
- Justice, C. O., et al. (1998), The Moderate Resolution Imaging Spectroradiometer (MODIS): Land remote sensing for global change research, *IEEE Trans. Geosci. Remote Sens.*, 36(4), 1228–1249, doi:10.1109/36.701075.
- Karl, T. R., and P. D. Jones (1989), Urban bias in area-averaged surface air temperature trends, *Bull. Am. Meteorol. Soc.*, 70(3), 265–270, doi:10.1175/1520-0477(1989)070<0265:ubaia>2.0.co;2.
- Karl, T. R., H. F. Diaz, and G. Kukla (1988), Urbanization: Its detection and effect in the United States climate record, *J. Clim.*, 1(11), 1099–1123, doi:10.1175/1520-0442(1988)001<1099:uidae>2.0.co;2.
- Kato, S., and Y. Yamaguchi (2007), Estimation of storage heat flux in an urban area using ASTER data, *Remote Sens. Environ.*, 110(1), 1–17, doi:10.1016/j.rse.2007.02.011.
- Kidder, S. Q., and H. T. Wu (1987), A multispectral study of the St. Louis area under snow-covered conditions using NOAA-7 AVHRR data, *Remote Sens. Environ.*, 22(2), 159–172, doi:10.1016/0034-4257(87)90056-3.
- Kribus, A., I. Vishnevetsky, E. Rotenberg, and D. Yakir (2003), Systematic errors in the measurement of emissivity caused by directional effects, *Appl. Opt.*, 42(10), 1839–1846, doi:10.1364/AO.42.001839.
- Kuang, W., Y. Dou, C. Zhang, W. Chi, A. Liu, Y. Liu, R. Zhang, and J. Liu (2015), Quantifying the heat flux regulation of metropolitan land use/land cover components by coupling remote sensing modeling with in situ measurement, *J. Geophys. Res. Atmos.*, 120, 113–130, doi:10.1002/2014JD022249.
- Laguarde, J. P., P. Moreau, M. Irvine, J. M. Bonnefond, J. A. Voogt, and F. Solliec (2004), Airborne experimental measurements of the angular variations in surface temperature over urban areas: Case study of Marseille (France), *Remote Sens. Environ.*, 93(4), 443–462, doi:10.1016/j.rse.2003.12.011.
- Laguarde, J. P., A. Henon, M. Irvine, J. Voogt, G. Pigeon, P. Moreau, V. Masson, and P. Mestayer (2012), Experimental characterization and modelling of the nighttime directional anisotropy of thermal infrared measurements over an urban area: Case study of Toulouse (France), *Remote Sens. Environ.*, 117, 19–33, doi:10.1016/j.rse.2011.06.022.
- Li, X., P. Gong, and L. Liang (2015), A 30-year (1984–2013) record of annual urban dynamics of Beijing City derived from Landsat data, *Remote Sens. Environ.*, 166, 78–90, doi:10.1016/j.rse.2015.06.007.
- Liu, G., Y. Wang, F. Hu, W. Zhang, and Y. Hu (2003), Observation of radiation grads by 320-meter meteorological tower in Beijing, *ACTA Energiae Solaris Sin.*, 24(3), 295–301.
- Liu, K., H. B. Su, X. K. Li, W. M. Wang, L. J. Yang, and H. Liang (2016), Quantifying spatial-temporal pattern of urban heat Island in Beijing: An improved assessment using land surface temperature (LST) time series observations From LANDSAT, MODIS, and Chinese New Satellite GaoFen-1, *IEEE J. Sel. Top. Appl. Earth Observ. Remote Sens.*, 9(5), 2028–2042, doi:10.1109/jstars.2015.2513598.
- Lowry, W. P. (1977), Empirical estimation of urban effects on climate: A problem analysis, *J. Appl. Meteorol.*, 16(2), 129–135, doi:10.1175/1520-0450(1977)016<0129:EEOUEO>2.0.CO;2.
- Lu, L., X. Zhang, K. Yu, W. Zhao, and L. Wang (2014), The realtime quality control and application to the data collected by Beijing automatic weather station network, *J. Anhui Agric. Sci.*, 42(16), 5153–5155.
- Lu, Y., Y. Xu, J. Ma, and W. Quan (2014), Quantitative assessment and planning simulation of Beijing urban heat island, *Ecol. Environ. Sci.*, 23(7), 1156–1163, doi:10.3969/j.issn.1674-5906.2014.07.010.
- McAtee, B. K., A. J. Prata, and M. J. Lynch (2003), The angular behavior of emitted thermal infrared radiation (8–12 μm) at a semiarid site, *J. Appl. Meteorol.*, 42(8), 1060–1071, doi:10.1175/1520-0450(2003)042<1060:TABOET>2.0.CO;2.
- Mertes, C. M., A. Schneider, D. Sulla-Menashe, A. J. Tatem, and B. Tan (2015), Detecting change in urban areas at continental scales with MODIS data, *Remote Sens. Environ.*, 158, 331–347, doi:10.1016/j.rse.2014.09.023.
- Mestayer, P. G., et al. (2005), The urban boundary-layer field campaign in Marseille (UBL/CLU-ESCOMPTE): Set-up and first results, *Bound. Layer Meteorol.*, 114(2), 315–365, doi:10.1007/s10546-004-9241-4.
- Meyers, T. P., and S. E. Hollinger (2004), An assessment of storage terms in the surface energy balance of maize and soybean, *Agri. For. Meteorol.*, 125(1–2), 105–115, doi:10.1016/j.agrformet.2004.03.001.
- Miao, S. G., J. X. Dou, F. Chen, J. Li, and A. G. Li (2012), Analysis of observations on the urban surface energy balance in Beijing, *Sci. China Earth Sci.*, 55(11), 1881–1890, doi:10.1007/s11430-012-4411-6.
- Muller, C. L., L. Chapman, C. S. B. Grimmond, D. T. Young, and X.-M. Cai (2013a), Toward a standardized metadata protocol for urban meteorological networks, *Bull. Am. Meteorol. Soc.*, 94(8), 1161–1185, doi:10.1175/bams-d-12-00096.1.
- Muller, C. L., L. Chapman, C. S. B. Grimmond, D. T. Young, and X. Cai (2013b), Sensors and the city: A review of urban meteorological networks, *Int. J. Climatol.*, 33(7), 1585–1600, doi:10.1002/joc.3678.

- Offerle, B., C. S. B. Grimmond, and K. Fortuniak (2005), Heat storage and anthropogenic heat flux in relation to the energy balance of a central European city centre, *Int. J. Climatol.*, 25(10), 1405–1419, doi:10.1002/joc.1198.
- Oke, T. R. (1973), City size and the urban heat island, *Atmos. Environ.*, 7(8), 769–779, doi:10.1016/0004-6981(73)90140-6.
- Oke, T. R. (1982), The Energetic basis of the urban heat island, *Q. J. R. Meteorol. Soc.*, 108(455), 1–24, doi:10.1002/qj.49710845502.
- Oke, T. R. (2008), Chapter 11: Urban observations, in *World Meteorological Organization, WMO No. 8 Guide to Meteorological Instruments and Observation Methods: Part II*, pp. 11–11–11–25, WMO, Geneva, Switzerland.
- Oke, T. R., and H. A. Cleugh (1987), Urban heat storage derived as energy balance residuals, *Boundary Layer Meteorol.*, 39(3), 233–245, doi:10.1007/bf00116120.
- Oke, T. R., G. T. Johnson, D. G. Steyn, and I. D. Watson (1991), Simulation of surface urban heat islands under 'ideal' conditions at night. Part 2: Diagnosis of causation, *Boundary Layer Meteorol.*, 56(4), 339–358, doi:10.1007/bf00119211.
- Parker, D. E. (2006), A demonstration that large-scale warming is not urban, *J. Clim.*, 19(12), 2882–2895, doi:10.1175/jcli3730.1.
- Parker, D. E. (2010), Urban heat island effects on estimates of observed climate change, *WIREs-Clim. Change*, 1(1), 123–133, doi:10.1002/wcc.0021.
- Peng, J., P. Xie, Y. Liu, and J. Ma (2016), Urban thermal environment dynamics and associated landscape pattern factors: A case study in the Beijing metropolitan region, *Remote Sens. Environ.*, 173, 145–155, doi:10.1016/j.rse.2015.11.027.
- Peng, S. S., S. L. Piao, P. Ciais, P. Friedlingstein, C. Ottle, F. M. Breon, H. J. Nan, L. M. Zhou, and R. B. Myneni (2012), Surface urban heat island across 419 global big cities, *Environ. Sci. Technol.*, 46(2), 696–703, doi:10.1021/es2030438.
- Peterson, T. C. (2003), Assessment of urban versus rural in situ surface temperatures in the contiguous United States: No difference found, *J. Clim.*, 16(18), 2941–2959, doi:10.1175/1520-0442(2003)016<2941:aouvr>2.0.co;2.
- Pielke, R., et al. (2007a), Unresolved issues with the assessment of multidecadal global land surface temperature trends, *J. Geophys. Res.*, 112, D24S08, doi:10.1029/2006JD008229.
- Pielke, R., et al. (2007b), Documentation of uncertainties and biases associated with surface temperature measurement sites for climate change assessment, *Bull. Am. Meteorol. Soc.*, 88(6), 913–928, doi:10.1175/bams-88-6-913.
- Price, J. C. (1979), Assessment of the urban heat island effect through the use of satellite data, *Mon. Weather Rev.*, 107(11), 1554–1557, doi:10.1175/1520-0493(1979)107<1554:aouhi>2.0.co;2.
- Pu, R., P. Gong, R. Michishita, and T. Sasagawa (2006), Assessment of multi-resolution and multi-sensor data for urban surface temperature retrieval, *Remote Sens. Environ.*, 104(2), 211–225, doi:10.1016/j.rse.2005.09.022.
- Ren, G., and Y. Zhou (2014), Urbanization effect on trends of extreme temperature indices of national stations over mainland China, 1961–2008, *J. Clim.*, 27(6), 2340–2360, doi:10.1175/jcli-d-13-00393.1.
- Rosenfeld, D. (2000), Suppression of rain and snow by urban and industrial air pollution, *Science*, 287(5459), 1793–1796, doi:10.1126/science.287.5459.1793.
- Roth, M., T. R. Oke, and W. J. Emery (1989), Satellite-derived urban heat island from three coastal cities and the utilization of such data in urban climatology, *Int. J. Climatol.*, 10(11), 1699–1720, doi:10.1080/01431168908904002.
- Rydin, Y., et al. (2012), Shaping cities for health: Complexity and the planning of urban environments in the 21st century, *Lancet*, 379(9831), 2079–2108, doi:10.1016/s0140-6736(12)60435-8.
- Sailor, D. J., M. Georgescu, J. M. Milne, and M. A. Hart (2015), Development of a national anthropogenic heating database with an extrapolation for international cities, *Atmos. Environ.*, 118, 7–18, doi:10.1016/j.atmosenv.2015.07.016.
- Sakakibara, Y., and K. Owa (2005), Urban-rural temperature differences in coastal cities: Influence of rural sites, *Int. J. Climatol.*, 25(6), 811–820, doi:10.1002/joc.1180.
- Sarrat, C., A. Lemonsu, V. Masson, and D. Guedalia (2006), Impact of urban heat island on regional atmospheric pollution, *Atmos. Environ.*, 40(10), 1743–1758, doi:10.1016/j.atmosenv.2005.11.037.
- Schneider, A., M. A. Friedl, and D. Potere (2009), A new map of global urban extent from MODIS satellite data, *Environ. Res. Lett.*, 4(4), 044003, doi:10.1088/1748-9326/4/4/044003.
- Schwarz, N., S. Lautenbach, and R. Seppelt (2011), Exploring indicators for quantifying surface urban heat islands of European cities with MODIS land surface temperatures, *Remote Sens. Environ.*, 115(12), 3175–3186, doi:10.1016/j.rse.2011.07.003.
- Smoliak, B. V., P. K. Snyder, T. E. Twine, P. M. Mykleby, and W. F. Hertel (2015), Dense network observations of the twin cities canopy-layer urban heat island, *J. Appl. Meteorol. Climatol.*, 54(9), 1899–1917, doi:10.1175/jamc-d-14-0239.1.
- Stewart, I. D. (2011), A systematic review and scientific critique of methodology in modern urban heat island literature, *Int. J. Climatol.*, 31(2), 200–217, doi:10.1002/joc.2141.
- Stewart, I. D., and T. R. Oke (2012), Local climate zones for urban temperature studies, *Bull. Am. Meteorol. Soc.*, 93(12), 1879–1900, doi:10.1175/BAMS-D-11-00019.1.
- Sun, H., Y. H. Chen, and W. F. Zhan (2015), Comparing surface- and canopy-layer urban heat islands over Beijing using MODIS data, *Int. J. Remote Sens.*, 36(21), 5448–5465, doi:10.1080/01431161.2015.1101504.
- Susaki, J., M. Kajimoto, and M. Kishimoto (2014), Urban density mapping of global megacities from polarimetric SAR images, *Remote Sens. Environ.*, 155, 334–348, doi:10.1016/j.rse.2014.09.006.
- Tan, J. G., L. M. Yang, C. S. B. Grimmond, J. P. Shi, W. Gu, Y. Y. Chang, P. Hu, J. Sun, X. Y. Ao, and Z. H. Han (2015), Urban integrated meteorological observations: Practice and experience in Shanghai, China, *Bull. Am. Meteorol. Soc.*, 96(1), 85–102, doi:10.1175/bams-d-13-00216.1.
- Theeuwes, N. E., G.-J. Steeneveld, R. J. Ronda, M. W. Rotach, and A. A. M. Holtslag (2015), Cool city mornings by urban heat, *Environ. Res. Lett.*, 10(11), doi:10.1088/1748-9326/10/11/114022.
- Tong, H., H. Liu, J. Sang, and F. Hu (2004), The impact of urban anthropogenic heat on Beijing heat environment, *Clim. Environ. Res.*, 9(3), 409–421.
- Voogt, J. A., and T. R. Oke (2003), Thermal remote sensing of urban climates, *Remote Sens. Environ.*, 86(3), 370–384, doi:10.1016/s0034-4257(03)00079-8.
- Wan, Z. M., and J. Dozier (1996), A generalized split-window algorithm for retrieving land-surface temperature from space, *IEEE Trans. Geosci. Remote Sens.*, 34(4), 892–905, doi:10.1109/36.508406.
- Wan, Z. M., Y. L. Zhang, Q. C. Zhang, and Z. L. Li (2002), Validation of the land-surface temperature products retrieved from Terra Moderate Resolution Imaging Spectroradiometer data, *Remote Sens. Environ.*, 83(1–2), 163–180, doi:10.1016/s0034-4257(02)00093-7.
- Wang, J., Q. Chang, and D. Liu (2014), The flowering phenophase response of early spring herb to the urbanization process in Beijing, *ACTA Ecol. Sin.*, 34(22), 6701–6710.
- Wang, J., C. C. Li, L. Y. Hu, Y. Y. Zhao, H. B. Huang, and P. Gong (2015), Seasonal land cover dynamics in Beijing derived from Landsat 8 data using a spatio-temporal contextual approach, *Remote Sens.*, 7(1), 865–881, doi:10.3390/rs70100865.

- Wang, K. C., and R. E. Dickinson (2012), A review of global terrestrial evapotranspiration: Observation, modeling, climatology, and climatic variability, *Rev. Geophys.*, 50, RG2005, doi:10.1029/2011RG000373.
- Wang, K. C., and S. Liang (2009), Evaluation of ASTER and MODIS land surface temperature and emissivity products using long-term surface longwave radiation observations at SURFRAD sites, *Remote Sens. Environ.*, 113(7), 1556–1565, doi:10.1016/j.rse.2009.03.009.
- Wang, K. C., Z. Wan, P. Wang, M. Sparrow, J. Liu, and S. Haginoya (2007a), Evaluation and improvement of the MODIS land surface temperature/emissivity products using ground-based measurements at a semi-desert site on the western Tibetan Plateau, *Int. J. Remote Sens.*, 28(11), 2549–2565, doi:10.1080/01431160600702665.
- Wang, K. C., J. Wang, P. Wang, M. Sparrow, J. Yang, and H. Chen (2007b), Influences of urbanization on surface characteristics as derived from the Moderate-Resolution Imaging Spectroradiometer: A case study for the Beijing metropolitan area, *J. Geophys. Res.*, 112, D22S06, doi:10.1029/2006JD007997.
- Wang, K. C., R. E. Dickinson, M. Wild, and S. Liang (2010a), Evidence for decadal variation in global terrestrial evapotranspiration between 1982 and 2002: 1. Model development, *J. Geophys. Res.*, 115, D20112, doi:10.1029/2010JD013847.
- Wang, K. C., R. E. Dickinson, M. Wild, and S. Liang (2010b), Evidence for decadal variation in global terrestrial evapotranspiration between 1982 and 2002: 2. Results, *J. Geophys. Res.*, 115, D20113, doi:10.1029/2010JD013847.
- Wang, X., L. Bian, and C. Lu (2003), A study of characteristic parameters of atmosphere boundary layer over Beijing in urban and suburban area in autumn, *Clim. Environ. Res.*, 8(4), 475–484.
- Weng, Q. H. (2009), Thermal infrared remote sensing for urban climate and environmental studies: Methods, applications, and trends, *ISPRS J. Photogramm. Remote Sens.*, 64(4), 335–344, doi:10.1016/j.isprsjprs.2009.03.007.
- Weng, Q. H., D. S. Lu, and J. Schubring (2004), Estimation of land surface temperature-vegetation abundance relationship for urban heat island studies, *Remote Sens. Environ.*, 89(4), 467–483, doi:10.1016/j.rse.2003.11.005.
- Wolfe, R. E., M. Nishihama, A. J. Fleig, J. A. Kuyper, D. P. Roy, J. C. Storey, and F. S. Patt (2002), Achieving sub-pixel geolocation accuracy in support of MODIS land science, *Remote Sens. Environ.*, 83(1–2), 31–49, doi:10.1016/s0034-4257(02)00085-8.
- Wood, C. R., et al. (2013), An overview of the urban boundary layer atmosphere network in Helsinki, *Bull. Am. Meteorol. Soc.*, 94(11), 1675–1690, doi:10.1175/bams-d-12-00146.1.
- Xu, Y. M., and Y. H. Liu (2015), Monitoring the near-surface urban heat island in Beijing, China by satellite remote sensing, *Geogr. Res.*, 53(1), 16–25, doi:10.1111/1745-5871.12092.
- Yan, W. Y., A. Shaker, and N. El-Ashmary (2015), Urban land cover classification using airborne LiDAR data: A review, *Remote Sens. Environ.*, 158, 295–310, doi:10.1016/j.rse.2014.11.001.
- Yang, P., W. Liu, J. Zhong, and J. Yang (2011), Evaluating the quality of temperature measured at automatic weather station in Beijing, *J. Appl. Meteorol. Sci.*, 22(6), 706–715.
- Yang, P., G. Y. Ren, and W. D. Liu (2013), Spatial and temporal characteristics of Beijing urban heat island intensity, *J. Appl. Meteorol. Climatol.*, 52(8), 1803–1816, doi:10.1175/jamc-d-12-0125.1.
- Zhao, L., X. Lee, R. B. Smith, and K. Oleson (2014), Strong contributions of local background climate to urban heat islands, *Nature*, 511(7508), 216–219, doi:10.1038/nature13462.
- Zhou, D., S. Zhao, L. Zhang, and S. Liu (2016), Remotely sensed assessment of urbanization effects on vegetation phenology in China's 32 major cities, *Remote Sens. Environ.*, 176, 272–281, doi:10.1016/j.rse.2016.02.010.
- Zhou, L., R. E. Dickinson, Y. Tian, J. Fang, Q. Li, R. K. Kaufmann, C. J. Tucker, and R. B. Myneni (2004), Evidence for a significant urbanization effect on climate in China, *Proc. Natl. Acad. Sci. U.S.A.*, 101(26), 9540–9544, doi:10.1073/pnas.0400357101.
- Zhou, W. Q., G. L. Huang, and M. L. Cadenasso (2011), Does spatial configuration matter? Understanding the effects of land cover pattern on land surface temperature in urban landscapes, *Landsc. Urban Plan.*, 102(1), 54–63, doi:10.1016/j.landurbplan.2011.03.009.